

Theory of spin current in chiral helimagnet

I. G. Bostrem,¹ Jun-ichiro Kishine,² and A. S. Ovchinnikov¹

¹*Department of Physics, Ural State University, Ekaterinburg, 620083 Russia, and*

²*Department of Basic Sciences, Kyushu Institute of Technology, Kitakyushu 804-8550, Japan*

(Dated: April 15, 2019)

We give detailed description of the transport spin current in the chiral helimagnet. Under the static magnetic field applied perpendicular to the helical axis, the magnetic kink crystal (chiral soliton lattice) is formed. Once the kink crystal begins to move under the Galilean boost, the spin-density accumulation occurs inside each kink and there emerges periodic arrays of the induced magnetic dipoles carrying the transport spin current. The coherent motion of the kink crystal is dynamically inducing the spontaneous demagnetization field. This mechanism is analogous to the Döring-Becker-Kittel mechanism of the domain wall motion in ferromagnets. To describe the kink crystal motion, we took account of not only the tangential φ -fluctuations but and the longitudinal θ -fluctuations around the helimagnetic configuration. Based on the collective coordinate method and the Dirac's canonical formulation for singular Lagrangian theory, we derived the closed formulae for the mass, spin current and induced magnetic dipole moment accompanied with the kink crystal motion. To materialize the theoretical model presented here, symmetry-adapted material synthesis would be required, where the interplay of crystallographic and magnetic chirality plays a key role there.

PACS numbers: Valid PACS appear here

I. INTRODUCTION

The core problem in the multidisciplinary field of spintronics is how to create, transport, and manipulate spin currents.¹ The key notions include the current-driven spin-transfer torque^{2,3,4,5,6} and resultant force acting on a domain wall (DW)^{7,8} in metallic ferromagnetic/nonmagnetic multilayers, the dissipationless spin currents in paramagnetic spin-orbit coupled systems,^{9,10,11} and magnon transport in textured magnetic structures.¹² A fundamental query behind the issue is how to describe transport spin currents.¹³ To make clear the meaning of the spin currents, we need to note the spin can appear in the macroscopic Maxwell equations only in the form of spin magnetization. In this viewpoint, the spin current is understood as the deviation of the spin projection from its equilibrium value. An emergence of the coherent collective transport in *non-equilibrium* state is then a manifestation of the dynamical off-diagonal long range order (DODLRO).¹⁴

On the other hand, the physical currents are classified into two categories, i.e., the gauge current originating from the gauge invariance and the inertial current originating from the Galilean invariance. The electric current is the gauge current, where the electric charge is coupled to the electromagnetic U(1) gauge field. The electromagnetic field is a physical gauge field that has its own dynamics, i.e., we know the electromagnetic field energy. Then, the charge current j_i and the charge density ρ are related via the continuity equation $\partial\rho/\partial t = -\partial j_i/\partial x_i$. On the other hand, a typical example of the inertial current is the momentum current in a classical ideal fluid, where the momentum current Π_{ij} satisfies the continuity equation, $\partial(\rho v_i)/\partial t = -\partial\Pi_{ij}/\partial x_j$, and given by $\Pi_{ij} = P\delta_{ij} + \rho v_i v_j$ with P being equilibrium pressure.¹⁵

The non-equilibrium current is described by $\rho v_i v_j$. In the spin current problem, at present, we have no known gauge field directly coupled to the spin current. Therefore, a promising candidate is the *inertial current of the magnetization*.

Historically, Döring¹⁶ pointed out that the longitudinal component of the slanted magnetic moment inside the Bloch DW emerges as a consequence of translational motion of the DW. An additional magnetic energy associated with the resultant demagnetization field is interpreted as the kinetic energy of the wall. This idea was simplified by Becker¹⁷ and Kittel.¹⁸ Recent progress of material synthesis sheds new light on this problem. In a series of magnets belonging to chiral space group without any rotoinversion symmetry elements, the crystallographic chirality gives rise to the asymmetric Dzyaloshinskii interaction that stabilizes either left-handed or right-handed chiral magnetic structures.¹⁹ In these chiral helimagnets, magnetic field applied perpendicular to the helical axis stabilizes a periodic array of DWs with definite spin chirality forming kink crystal or chiral soliton lattice.²⁰

We recently proposed a new way to generate a spin current in the chiral helimagnets with magnetic field applied in the plain of rotation of magnetization.²¹ The mechanism is quite analogous to the Döring-Becker-Kittel mechanism. We showed that the periodic spin accumulation occurs as a dynamical effect caused by the moving magnetic kink crystal (chiral soliton lattice) formed in the chiral helimagnet under the static magnetic field applied perpendicular to the helical axis. The current is inertial flow triggered by the Galilean boost of the kink crystal. An emergence of the transport magnetic currents is then a consequence of the dynamical off-diagonal long range order along the helical axis.

In this paper, we give a full account of the results sum-

marized in Ref.²¹. In Sec. II, we give an overview of basic properties of the chiral magnets that materialize the theoretical model considered in this paper. In Sec. III, we give a theoretical model and present standard description on the kink crystal formation. In Sec. IV, the vibrational modes around the kink crystal state are analyzed. These modes are simply phonon modes around the kink crystal state. In Sec. V, we apply the collective coordinate method to the moving kink crystal and accomplish the Dirac's canonical formulation for singular Lagrangian theory. Through this analysis, it is possible to make clear the physical meaning of the mass carried by the moving kink crystal. In Sec. VI, we introduce the transport magnetic current and give its analytic form in the weak field limit. In Sec. VII, we perform numerical estimates of the mass, magnetic current, and magnetization induced by the moving kink crystal. In Sec. VIII, we discuss issues closely related to the present problem, including the background spin current problem, spin supercurrent in the superfluid ³He, and experimental aspects of our effects. Finally, we summarize the paper in Sec. IX.

II. CHIRAL HELIMAGNET

In this section, we briefly review basic properties of chiral helimagnets that materialize our theoretical model. Recent progress of material synthesis promotes systematic researches on a series of magnets belonging to chiral space group without any rotoinversion symmetry elements.²⁰ In the chiral magnets, the crystallographic chirality possibly gives rise to the asymmetric Dzyaloshinskii interaction that stabilizes the chiral helimagnetic structure, where either left-handed or right-handed magnetic chiral helix is formed.¹⁹ As we will see, in the chiral helimagnets, magnetic field applied perpendicular to the helical axis stabilizes a periodic array of DWs with definite spin chirality forming kink crystal or chiral soliton lattice.²⁰

The chiral helimagnetic structure is an incommensurate magnetic structure with a single propagation vector $\mathbf{k}_0 = (0, 0, k)$. The space group \mathcal{G} consists of the elements $\{g_i\}$. Among them, some elements leave the propagation vector $\mathbf{k}_0 = (0, 0, k)$ invariant, i.e., these elements form the little group $G_{\mathbf{k}_0}$.^{22,23} The magnetic representation²³ Γ_{mag} is written as $\Gamma_{mag} = \Gamma_{perm} \otimes \Gamma_{axial}$, where Γ_{perm} and Γ_{axial} represent the Wyckoff permutation representation and the axial vector representation, respectively. Then, Γ_{mag} is decomposed into the non-zero irreducible representations of $G_{\mathbf{k}_0}$. The incommensurate magnetic structure is determined by a "magnetic basis frame" of an axial vector space and the propagation vector \mathbf{k} . In specific magnetic ion, the decomposition becomes $\Gamma_{mag} = \sum_i n_i \Gamma_i$, where Γ_i is the irreducible representations of $G_{\mathbf{k}_0}$. Then, we have two cases leading to the chiral helimagnetic magnetic structure. Case I: The magnetic moments are described by two independent one-dimensional representations that

form two-dimensional basis frames, or Case II: The magnetic moments are described by a single two-dimensional representations that form two-dimensional basis frames. In these cases, the symmetry condition allows the chiral helimagnetic structure to be realized. Then, the structure is stabilized by the generalized Dzyaloshinskii interaction. The generalized Dzyaloshinskii interaction means symmetry-adapted anti-symmetric exchange interaction, not restricted to conventional Dzyaloshinskii-Moriya (DM) interaction caused by the on-site spin-orbit coupling and the inter-site exchange interactions. The presence of this term is justified by the existence of the Lifshitz invariant²⁹ for the little group $G_{\mathbf{k}_0}$.

Typically, in the case of the inorganic chiral magnets, the crystal packing is close, the exchange interaction is rather strong, and consequently the transition temperature T_c is higher. As examples of the inorganic chiral helimagnets, $\text{Cr}_{1/3}\text{NbS}_2$ ($T_c = 120\text{K}$) belongs to the hexagonal space group $P6_322$ ($a = 5.75\text{\AA}$, $c = 12.12\text{\AA}$).²⁴ The copper metatopate, CuB_2O_4 ($T_c = 10\text{K}$) has a larger unit cell and belongs to the tetragonal space group $I\bar{4}2d$ ($a = 11.48\text{\AA}$, $c = 5.620\text{\AA}$).^{25,26} On the other hand, in the case of the molecular-based chiral magnets, the crystal packing is usually loose, the exchange interaction is rather weak, and consequently T_c is lower. As examples of molecular-based magnets, the structurally characterized green needle, $[\text{Cr}(\text{CN})_6][\text{Mn}(S \text{ or } R)\text{-pnH}(\text{H}_2\text{O})]\text{H}_2\text{O}$ ($T_c = 38\text{K}$), belongs to the orthorhombic space group $P2_12_12_1$ ($a = 7.628\text{\AA}$, $b = 14.51\text{\AA}$, $c = 14.93\text{\AA}$). The yellow needle, $\text{K}_{0.4}[\text{Cr}(\text{CN})_6][\text{Mn}(S)\text{-pn}](S)\text{-pnH}_{0.6}$: ((S)-pn = (S)-1,2-diaminopropane) ($T_c = 53\text{K}$), belongs to the hexagonal space group $P6_1$ ($a = 14.77\text{\AA}$, $c = 17.57\text{\AA}$).²⁰ From the symmetry-based viewpoints, these space groups are all eligible to realize the chiral helimagnetic order.

III. FORMATION OF THE KINK CRYSTAL

As shown in Fig. 1, we consider a system of the chiral helimagnetic chains described by the model Hamiltonian

$$\mathcal{H} = -J \sum_{\langle i,j \rangle} \mathbf{S}_i \cdot \mathbf{S}_j + \mathbf{D} \cdot \sum_{\langle i,j \rangle} \mathbf{S}_i \times \mathbf{S}_j - \tilde{\mathbf{H}} \cdot \sum_i \mathbf{S}_i, \quad (1)$$

where the first term represents the ferromagnetic coupling with the strength $J > 0$ between the nearest neighbor spins \mathbf{S}_i and \mathbf{S}_j . The second term represents the parity-violating Dzyaloshinskii interaction between the nearest neighbors, characterized by the the mono-axial vector $\mathbf{D} = D\hat{\mathbf{e}}_x$ along a certain crystallographic chiral axis (taken as the x -axis). The third term is the Zeeman coupling with the magnetic field $\tilde{\mathbf{H}} = g\mu_B H\hat{\mathbf{e}}_y$ applied *perpendicular* to the chiral axis. When we treat the model Hamiltonian (1), we implicitly assume that the

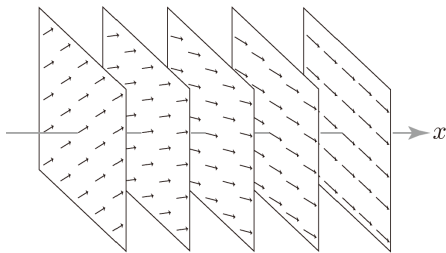


FIG. 1: Schematic view of the model chiral helimagnet considered here.

magnetic atoms form a cubic lattice and the uniform ferromagnetic coupling exists between the adjacent chains to stabilize the long-range order. Then, the Hamiltonian (1) is interpreted as a quasi one-dimensional model based on the interchain mean field picture.²⁸

When $H = 0$, the long-period incommensurate helimagnetic structure is stabilized with the definite chirality (left-handed or right-handed) fixed by the direction of the mono-axial \mathbf{D} -vector. The Hamiltonian (1) is the same as the model treated by Liu²⁷ except that we ignore the single-ion anisotropy energy. Once we take into account the easy-axis type anisotropy term, $-K \sum_i (S_i^x)^2$, the mean field ground state configuration becomes either the chiral helimagnet for $K < D^2/J$, or the Ising ferromagnet for $K > D^2/J$. In this paper, we assume $K = 0$ and left an effect of K for a future study.

Taking the semiclassical parametrization of Heisenberg spins in the continuum limit $\mathbf{S}(x) = S(\cos \theta(x), \sin \theta(x) \cos \varphi(x), \sin \theta(x) \sin \varphi(x))$ by using the slowly varying polar angles $\theta(x)$ and $\varphi(x)$ [see Fig. 2(a)], the Hamiltonian acquires the form

$$\begin{aligned} \mathcal{H}[\varphi(x), \theta(x)] &= JS^2 \int_0^L dx \left[\frac{1}{2} \{\partial_x \theta(x)\}^2 + \frac{1}{2} \sin^2 \theta \{\partial_x \varphi(x)\}^2 \right. \\ &\quad \left. - q_0 \sin^2 \theta(x) \partial_x \varphi(x) - m^2 \sin \theta(x) \cos \varphi(x) \right]. \quad (2) \end{aligned}$$

where

$$m = \sqrt{\frac{\tilde{H}}{JS}},$$

and L denotes the linear dimension of the system. From now on, all distances are measured in the lattice unit a_0 . The helical pitch in the zero field ($m = 0$) is given by $q_0 = D/J$.

The magnetic kink crystal phase is described by the stationary soliton solution, $\theta = \pi/2$ and $\varphi(x) = \varphi_0(x)$, where the stationary solution $\varphi_0(x)$ is found by analyzing $\mathcal{H}[\varphi_0(x), \theta(x) = \pi/2]$. Stationary condition $\delta\mathcal{H} = 0$ yields the sine-Gordon equation, $\varphi_{xx}(x) = m^2 \sin \varphi$, that produces a solution,

$$\cos \left[\frac{\varphi_0(x)}{2} \right] = \text{sn} \left[\frac{m}{\kappa} x, \kappa \right], \quad (3)$$

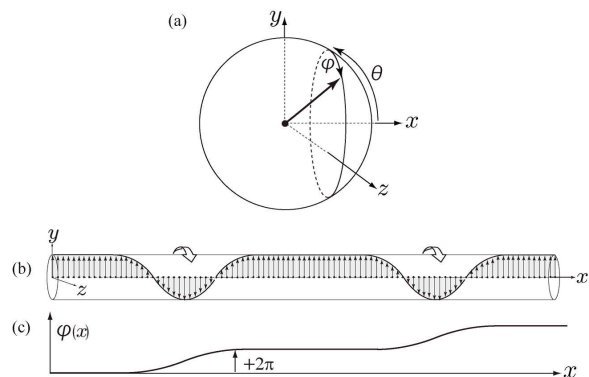


FIG. 2: (a) Polar coordinates in the laboratory frame. (b) Formation of the magnetic kink crystal in the chiral helimagnets under the transverse magnetic field, and (c) concomitant phase modulation. In (b), we depict a linear array of the spins along one chiral axis that is ferromagnetically coupled to the neighboring arrays.

where sn is the Jacobi elliptic function with the elliptic modulus κ ($0 < \kappa^2 < 1$). This solution corresponds to a periodic regular array of the magnetic kinks²⁹ with the "topological charge" density $\partial_x \varphi_0(x) = 2 \frac{m}{\kappa} \text{dn} \left(\frac{m}{\kappa} x, \kappa \right)$ and the period

$$\ell_{\text{kink}} = \frac{2\kappa K(\kappa)}{m}. \quad (4)$$

The kink corresponds to the phase winding in the left-handed ($\Delta\varphi = +2\pi$) or right-handed ($\Delta\varphi = -2\pi$) manners. Due to a presence of the uniform mono-axial Dzyaloshinskii vector \mathbf{D} , the kink with only positive (left-handed) or negative (right-handed) charge are energetically favored. The kink with the same charges repel each other, just like in the case of the Coulomb repulsion, and, as consequence, the magnetic kink crystal (soliton lattice) is formed as shown in Figs. 2(b) and (c). The energy per unit length \mathcal{E} is computed as a function of the elliptic modulus κ ,

$$\mathcal{E}(\kappa) = 2JS^2 m^2 \left(\frac{2E(\kappa)}{\kappa^2 K(\kappa)} - \frac{\pi q_0}{2m\kappa K(\kappa)} - \frac{1}{\kappa^2} + 1 \right), \quad (5)$$

where $K(\kappa)$ and $E(\kappa)$ denote the elliptic integrals of the first and second kind, respectively. Now, the condition $d\mathcal{E}/d\kappa = 0$ leads to $\kappa/m = 4E(\kappa)/\pi q_0$ that gives

$$\frac{1}{q_0} \sqrt{\frac{\tilde{H}}{JS}} = \frac{\pi}{4} \frac{\kappa}{E(\kappa)}, \quad (6)$$

where the r.h.s is a monotonously increasing function of κ . Using $\pi\kappa/4E(\kappa) \simeq \kappa/2 + \mathcal{O}(\kappa^2)$, in the case of weak field the elliptic modulus κ is given by

$$\kappa \simeq \frac{2}{q_0} \sqrt{\frac{\tilde{H}}{JS}}.$$

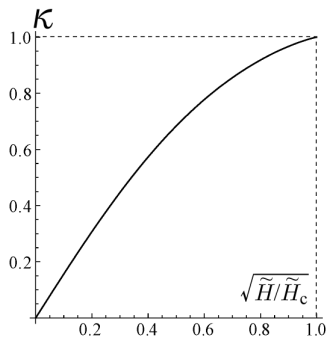


FIG. 3: The elliptic modulus κ is shown as a function of $\sqrt{\tilde{H}/\tilde{H}_c}$

From Eq.(6) one sees the period is given by

$$\ell_{\text{kink}} = \frac{8K(\kappa)E(\kappa)}{\pi q_0}. \quad (7)$$

We see that the period increases from $2\pi/q_0$ to infinity as κ increases from zero to unity. In the limit of $\kappa \rightarrow 0$, the sn function approaches sin and we have $\kappa/m \rightarrow 2/q_0$. Therefore, due to Eq.(3) we retain $\varphi_0(x) = q_0 x$ in the case of zero field.

In the Hamiltonian (2), the exchange processes favor the incommensurate (IC) chiral helimagnetic order, while the Zeeman term favors the commensurate (C) phase. The C-IC transition occurs at $\kappa = 1$ [$E(1) = 1$], and the critical value of m is given by, $\pi q_0/4m_c = 1$. The critical field strength \tilde{H}_c gives

$$\sqrt{\frac{\tilde{H}}{\tilde{H}_c}} = \frac{\kappa}{E(\kappa)}. \quad (8)$$

In Fig. 3, we show the relation of the elliptic modulus κ and the scaled field strength $\sqrt{\tilde{H}/\tilde{H}_c}$.

The magnetization density is computed as

$$\begin{aligned} M(x, \kappa) &= 2\mu_B S \cos \varphi_0(x) \\ &= 2\mu_B S \left\{ 1 - \frac{2}{\kappa^2} + \frac{2}{\kappa^2} \text{dn}^2 \left(\frac{m}{\kappa} x, \kappa \right) \right\}. \end{aligned} \quad (9)$$

An average of the magnetization is given by

$$\begin{aligned} \bar{M}(\kappa) &= \frac{1}{\ell_{\text{kink}}} \int_0^{\ell_{\text{kink}}} M(x) dx \\ &= 2\mu_B S \left(1 - \frac{2}{\kappa^2} + \frac{2E(\kappa)}{\kappa^2 K(\kappa)} \right). \end{aligned} \quad (10)$$

Upon decreasing temperatures, the effective spin length, S , is expected to grow in a mean field manner, and eventually the exchange terms (favoring the IC-phase) dominates the Zeeman term at the critical temperature $T = T_c$ given by $\pi q_0/4m(T_c) = 1$. Therefore, at constant temperature, the scaling law, $M(T, H_c) \propto H_c$, holds. This behavior is actually observed in the chiral helimagnet CuB_2O_4 .²⁶

IV. VIBRATIONAL MODES AROUND THE KINK-CRYSTAL STATE

Next, we consider the fluctuations around the kink crystal state. In this section, it is convenient to work with the dimensionless coordinate

$$\bar{x} = \frac{m}{\kappa} x = 2K(\kappa) \frac{x}{\ell_{\text{kink}}} = \frac{\pi}{4E(\kappa)} q_0 x. \quad (11)$$

We introduce $\bar{L} = mL/\kappa$ and $\bar{q}_0 = \kappa q_0/m$, and write the Hamiltonian (2) as

$$\mathcal{H} = JS^2 \frac{m}{\kappa} \bar{\mathcal{H}} = JS^2 \frac{2K(\kappa)}{\ell_{\text{kink}}} \bar{\mathcal{H}}, \quad (12)$$

where the dimensionless Hamiltonian $\bar{\mathcal{H}}$ is defined by

$$\bar{\mathcal{H}} = \int_0^{\bar{L}} d\bar{x} \left[\frac{1}{2} \{ \partial_{\bar{x}} \theta(\bar{x}) \}^2 + \frac{1}{2} \sin^2 \theta(\bar{x}) \{ \partial_{\bar{x}} \varphi(\bar{x}) \}^2 - \bar{q}_0 \sin^2 \theta(\bar{x}) \partial_{\bar{x}} \varphi(\bar{x}) - \kappa^2 \sin \theta(\bar{x}) \cos \varphi(\bar{x}) \right]. \quad (13)$$

Eqs. (3) and (6) are simply written as $\cos[\varphi_0(\bar{x})/2] = \text{sn}(\bar{x}, \kappa)$, and $\bar{q}_0 = 4E(\kappa)/\pi$, respectively. As the magnetic field increases from $H = 0$ to $H = H_c$, the elliptic modulus increases from $\kappa = 0$ to $\kappa = 1$. Then, the parameter \bar{q}_0 monotonously decreases from $\bar{q}_0 = 2$ to $\bar{q}_0 = 4/\pi \simeq 1.273$. The fluctuations consist of the vibrational (phonon) modes and the translational mode, that are separately treated. In this section, we examine the

phonon modes. We write

$$\varphi(\bar{x}) = \varphi_0(\bar{x}) + v(\bar{x}), \quad \theta(\bar{x}) = \frac{\pi}{2} + u(\bar{x}) \quad (14)$$

and expanding (13) up to u^2 and v^2 . Then we have $\bar{\mathcal{H}} = \int_0^{\bar{L}} d\bar{x} (\bar{\mathcal{H}}_0 + \bar{\mathcal{H}}_u + \bar{\mathcal{H}}_v + \bar{\mathcal{H}}_{\text{int}}) + \mathcal{O}(u^2, v^2)$, where $\bar{\mathcal{H}}_0$ corresponds to the stationary solution. The interaction part contains $-u^2(\partial_{\bar{x}} v)^2/2$ and u^4 terms that are neglected here. The vibrational term $\mathcal{V} = \int_0^{\bar{L}} d\bar{x} (\bar{\mathcal{H}}_u + \bar{\mathcal{H}}_v)$

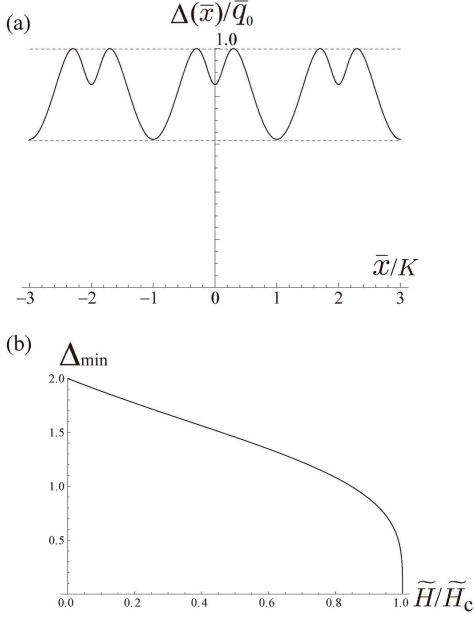


FIG. 4: (a) Spatial variation of the gap function $\Delta(\bar{x})$ for the θ -mode. (b) The minimum gap Δ_{\min} is shown as a function of \tilde{H}/\tilde{H}_c .

is given by $\overline{\mathcal{H}}_u = u\hat{\mathcal{L}}_u u$, and $\overline{\mathcal{H}}_v = v\hat{\mathcal{L}}_v v$, where the differential operators, $\hat{\mathcal{L}}_v$ and $\hat{\mathcal{L}}_u$, are defined by

$$\begin{cases} \hat{\mathcal{L}}_v = -\frac{1}{2}\partial_{\bar{x}}^2 + \frac{1}{2}\kappa^2 \cos \varphi_0, \\ \hat{\mathcal{L}}_u = -\frac{1}{2}\partial_{\bar{x}}^2 + \frac{1}{2}\kappa^2 \cos \varphi_0 + \frac{1}{2}\Delta(\bar{x})^2. \end{cases} \quad (15)$$

The "gap function" is defined by

$$\begin{aligned} \Delta(\bar{x}) &= \sqrt{2\bar{q}_0(\partial_{\bar{x}}\varphi_0)^2 - (\partial_{\bar{x}}\varphi_0)^2} \\ &= 2\sqrt{\bar{q}_0 \operatorname{dn}^2(\bar{x}, \kappa) - \operatorname{dn}^2(\bar{x}, \kappa)}, \end{aligned} \quad (16)$$

where the relation $\partial_{\bar{x}}\varphi_0 = 2\operatorname{dn}(\bar{x}, \kappa)$ was used. The minimum and maximum value of the gap are given by

$$\Delta_{\max} = \bar{q}_0, \quad \Delta_{\min} = \Delta(K) = 2\sqrt{\kappa'}\sqrt{\bar{q}_0 - \kappa'}, \quad (17)$$

respectively, where $\kappa' = \sqrt{1 - \kappa^2}$ is the complementary modulus. We see that the gap closes at the C-IC transition. In Fig.4 (a), we show the spatial variation of the gap function. The κ dependence of the minimum gap is shown in Fig.4 (b). For small κ , we have $\Delta_{\max} \simeq 2 - \kappa^2/2 - 3\kappa^4/32$, and $\Delta_{\min} \simeq 2 - \kappa^2/2 - 7\kappa^4/32$. Therefore, $\Delta_{\max}/\Delta_{\min} \simeq 1$ and it is appropriate to approximate $\Delta(\bar{x}) \simeq 2$ for the case of weak field. This approximation amounts to approximating $\operatorname{dn}(\bar{x}, \kappa) \simeq 1$.

If we considered only the tangential φ -mode, our problem reduces to the case first investigated by Sutherland.³⁰ Furthermore, the φ -mode is fully studied in the context

of the chiral helimagnet.^{31,32} In the present work, as we will see, it is essential to take account of not only the φ -mode but the θ -mode to realize the longitudinal magnetic current. In the case of zero-field, $\kappa = 0$, we have $\hat{\mathcal{L}}_v = -\frac{1}{2}\partial_{\bar{x}}^2$, and $\hat{\mathcal{L}}_u = -\frac{1}{2}\partial_{\bar{x}}^2 + \frac{1}{2}\bar{q}_0^2$. Therefore we see that θ -mode acquires the energy gap $(JS^2)(m/\kappa)\bar{q}_0 = DS^2$. On the other hand, the φ -mode becomes massless, because the φ -mode is the massless Goldstone mode corresponding to rigid rotation of the whole helix around the helical axis.³³ The θ -gap directly originates from the Dzyaloshinskii interaction that plays a role of easy plane anisotropy. Even after switching the perpendicular field, the θ -mode (φ -mode) remains to be massive (massless). The mode expansion is

$$v(\bar{x}) = \sum_{\alpha} \eta_{\alpha} v_{\alpha}(\bar{x}), \quad u(\bar{x}) = \sum_{\alpha} \xi_{\alpha} u_{\alpha}(\bar{x}), \quad (18)$$

where the basis $v_{\alpha}(\bar{x})$ and $u_{\alpha}(\bar{x})$ are determined through the eigenvalue equations,

$$\hat{\mathcal{L}}_v v_{\alpha}(\bar{x}) = \rho_{\alpha} v_{\alpha}(\bar{x}), \quad \hat{\mathcal{L}}_u u_{\alpha}(\bar{x}) = \lambda_{\alpha} u_{\alpha}(\bar{x}), \quad (19)$$

with a mode index α . The basis functions satisfy the orthonormal condition, $\int_0^{\bar{L}} d\bar{x} v_{\alpha}(\bar{x})v_{\beta}(\bar{x}) = \delta_{\alpha\beta}$ and $\int_0^{\bar{L}} d\bar{x} u_{\alpha}(\bar{x})u_{\beta}(\bar{x}) = \delta_{\alpha\beta}$. The vibrational part is now given by

$$\mathcal{V} = \int_0^{\bar{L}} d\bar{x} (\overline{\mathcal{H}}_u + \overline{\mathcal{H}}_v) = \sum_{\alpha} (\rho_{\alpha}\eta_{\alpha}^2 + \lambda_{\alpha}\xi_{\alpha}^2). \quad (20)$$

Eqs (19) reduce to the Schrödinger-type equations,

$$\frac{d^2 v_{\alpha}(\bar{x})}{d\bar{x}^2} = [2\kappa^2 \operatorname{sn}^2(\bar{x}, \kappa) - (\kappa^2 + 2\rho_{\alpha})]v_{\alpha}(\bar{x}), \quad (21)$$

$$\frac{d^2 u_{\alpha}(\bar{x})}{d\bar{x}^2} = [2\kappa^2 \operatorname{sn}^2(\bar{x}, \kappa) - (\kappa^2 - 4\bar{q}_0 + 4 + 2\lambda_{\alpha})]u_{\alpha}(\bar{x}). \quad (22)$$

In Eq. (22) we consider the case of weak field corresponding to small κ that admit of $\operatorname{dn}(\bar{x}, \kappa) \simeq 1$. In appendix A, we present the general scheme to treat the periodic potential having the spatial period $2K$ and show that this approximation does not affect qualitative result presented below. Now, both equations (22) and (21) reduce to the Jacobi form of the Lamé equation,³⁴

$$\frac{d^2 \Lambda(\bar{x})}{d\bar{x}^2} = [\ell(\ell + 1)\kappa^2 \operatorname{sn}^2(\bar{x}, \kappa) - \kappa^2(1 + A)]\Lambda(\bar{x}),$$

with $\ell = 1$. In appendix A, we gave a brief introduction to the Lamé equation. The spectrum A and solution $\Lambda(\bar{x})$ are parameterized by a single complex parameter α and given by,^{30,31}

$$A_{\alpha} = \frac{1}{\kappa^2} \operatorname{dn}^2 \alpha, \quad (23)$$

and

$$\Lambda_\alpha(\bar{x}) = N(\alpha) \frac{\vartheta_4\left(\frac{\pi}{2K}(\bar{x} - \bar{x}_0)\right)}{\vartheta_4\left(\frac{\pi}{2K}\bar{x}\right)} e^{-iQ\bar{x}}, \quad (24)$$

respectively, where $N(\alpha)$ is a normalization factor, \bar{x}_0 is a parameter depending on α , ϑ_i ($i = 1, 2, 3, 4$) denote the Theta functions,³⁴ and K' does the complete elliptic integral of the first kind with the complementary modulus $\kappa' = \sqrt{1 - \kappa^2}$. The representation (24) was given by Izyumov and Laptev,³¹ and differs from a conventional representation.^{30,34}

The Floquet index, corresponding to the wave number, is given by

$$Q_\alpha = \frac{\pi}{2K} + iZ(\alpha, \kappa), \quad (25)$$

where Z denotes the Jacobi's Zeta-function.³⁴ A dispersion relation is given by A as a function of Q . Possible region for α is determined through the condition that the Floquet index Q_α must be real, then Eq.(24) represents a propagating Bloch wave. This condition imposes α to belong to two segments on the complex α plane, the "acoustic" segment $\alpha = ia - iK' + K \in (K - 2iK', K]$ and the "optical" segment $\alpha = ia - iK' \in (-2iK', 0]$ with a being a *real* parameter running over the region $-K' < a \leq K'$. Corresponding \bar{x}_0 are given by $ia + K$ and ia for the acoustic and optic modes, respectively. Furthermore imposing the periodic boundary condition $\Lambda_\alpha(\bar{x} + \bar{L}) = \Lambda_\alpha(\bar{x})$, the quasi-momentum is introduced as usual, $Q = 2\pi n/\bar{L}$. Then, the energy dispersion consists of two branches, i.e., *the acoustic branch*,

$$\begin{cases} A_a^{(-)} = \frac{\kappa'^2}{\kappa^2} \text{sn}^2(a, \kappa'), \\ Q_a^{(-)} = \frac{\pi a}{2KK'} + Z(a, \kappa'), \end{cases} \quad (26)$$

and *the optical branch*,

$$\begin{cases} A_a^{(+)} = \frac{1}{\kappa^2 \text{sn}^2(a, \kappa')}, \\ Q_a^{(+)} = \frac{\pi a}{2KK'} + Z(a, \kappa') + \text{dn}(a, \kappa') \frac{\text{cn}(a, \kappa')}{\text{sn}(a, \kappa')}. \end{cases} \quad (27)$$

Where the real parameter a runs over $K' < a \leq K'$, the acoustic and optical branches are characterized by

$$0 \leq A_a^{(-)} < \frac{\kappa'^2}{\kappa^2}, \text{ for } 0 \leq |Q_a^{(-)}| \leq \frac{\pi}{2K},$$

and

$$\frac{1}{\kappa^2} \leq A_a^{(+)} < \infty, \text{ for } \frac{\pi}{2K} \leq |Q_a^{(-)}|,$$

respectively. Consequently, both the φ and ϑ mode consist of two bands,³⁰ i.e.,

$$\begin{cases} \text{Acoustic } \varphi \text{ mode :} \\ \omega_\varphi^{(-)} = \sqrt{\rho_a^{(-)}} = \frac{\kappa'}{\sqrt{2}} |\text{sn}(a, \kappa')|, \\ \text{Optical } \varphi \text{ mode :} \\ \omega_\varphi^{(+)} = \sqrt{\rho_a^{(+)}} = \frac{1}{\sqrt{2} |\text{sn}(a, \kappa')|}, \end{cases} \quad (28)$$

$$\begin{cases} \text{Acoustic } \vartheta \text{ mode :} \\ \omega_\vartheta^{(-)} = \sqrt{\lambda_a^{(-)}} = \sqrt{2\bar{q}_0 - 2 + \frac{\kappa'^2}{2} \text{sn}^2(a, \kappa')}, \\ \text{Optical } \vartheta \text{ mode :} \\ \omega_\vartheta^{(+)} = \sqrt{\lambda_a^{(+)}} = \sqrt{2\bar{q}_0 - 2 + \frac{1}{2\text{sn}^2(a, \kappa')}}. \end{cases} \quad (29)$$

We show the excitation spectrum ω_φ and ω_ϑ as functions of Q in Fig. 5. Because $4/\pi < \bar{q}_0 \leq 2$, the energy gap of the ϑ mode, $\Delta_\vartheta(a=0) = \sqrt{2\bar{q}_0 - 2}$, has a range $\sqrt{8/\pi - 2} < \Delta \leq \sqrt{2}$. The gap has a maximum value $\Delta_\vartheta = \sqrt{2}$ at zero field ($\kappa = 0$) and monotonously decreases as the field increases up to the critical field ($\kappa = 1$). Using the relations,³⁴

$$\vartheta_4\left(\frac{\pi}{2K}(\bar{x} - K)\right) = \vartheta_3\left(\frac{\pi}{2K}\bar{x}\right),$$

and

$$\text{dn}(\bar{x}, \kappa) = \sqrt{\kappa'} \frac{\vartheta_3\left(\frac{\pi}{2K}\bar{x}\right)}{\vartheta_4\left(\frac{\pi}{2K}\bar{x}\right)},$$

we have the normalized wave function at the bottom of the acoustic band as

$$\Lambda_{\alpha=0}(\bar{x}) = \sqrt{\frac{K(\kappa)}{E(\kappa)\bar{L}}} \text{dn}(\bar{x}, \kappa) = \frac{1}{2} \sqrt{\frac{K(\kappa)}{E(\kappa)\bar{L}}} \partial_{\bar{x}} \varphi_0(\bar{x}). \quad (30)$$

We see that $\Lambda_{\alpha=0}(\bar{x})$ exactly corresponds to the zero mode as discussed in the next section.

V. GALILEAN BOOST OF THE KINK CRYSTAL: COLLECTIVE COORDINATE METHOD AND DIRAC'S CANONICAL FORMULATION FOR SINGULAR LAGRANGIAN THEORY

In the previous section, we determined the phonon modes. Next we consider the translational mode. The translational symmetry broken by the kink formation gives rise to the Goldstone mode, i.e. zero mode $\partial_{\bar{x}} \varphi_0(\bar{x}) = 2\text{dn}(\bar{x}, \kappa)$. Although the Gaussian fluctuations around the kink crystal state are assumed to be small, this is not true for the zero mode which describes fluctuations without damping. Then, the center of mass

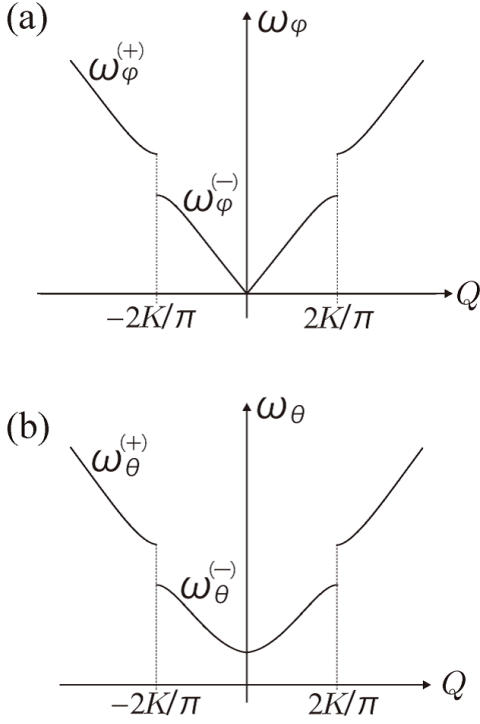


FIG. 5: The energy dispersions of the eigenmodes for (a) the tangential φ -fluctuation (ω_φ) and (b) the longitudinal θ -fluctuations (ω_θ).

coordinate is elevated to the status of the dynamical variable $X(t)$ and the phonon modes are orthogonal to the zero mode. To describe this situation, we follow the collective coordinate method.^{35,36}

At first, we construct the Lagrangian for the kink crystal system. We make use of the coherent states of spins,

$$|\mathbf{n}_i\rangle = \exp[i\theta_i \lambda \cdot \mathbf{S}] |S, S\rangle, \quad (31)$$

where

$$\lambda = \frac{\mathbf{n}_0 \times \mathbf{n}_i}{|\mathbf{n}_0 \times \mathbf{n}_i|}, \quad (32)$$

with $\mathbf{n}_i = (\cos \theta_i, \sin \theta_i \cos \varphi_i, \sin \theta_i \sin \varphi_i)$ and $\mathbf{n}_0 = (1, 0, 0)$. $S_i (i = x, y, z)$ are the generators of SU(2) in the spin- s representation and satisfy $[S_\alpha, S_\beta] = i\epsilon_{\alpha\beta\gamma} S_\gamma$. The highest weight state $|S, S\rangle$ satisfies $S_i^+ |S, S\rangle = S |S, S\rangle$ and $\mathbf{S}^2 |S, S\rangle = S(S+1) |S, S\rangle$. The states $|\mathbf{n}_i\rangle$ form an overcomplete set and give $\langle \mathbf{n}_i | \mathbf{S} | \mathbf{n}_i \rangle = S \mathbf{n}_i$. Using this representation, the Berry phase contribution to the real-time Lagrangian per unit area is written as

$$\begin{aligned} \mathcal{L}_{\text{Berry}} &= \hbar S \sum_i (\cos \theta_i - 1) \partial_t \varphi_i \\ &= \hbar S \frac{\kappa}{m} \int_0^{\bar{L}} d\bar{x} (\cos \theta - 1) \partial_t \varphi, \end{aligned} \quad (33)$$

where we took the continuum limit in the second line. Now, we construct the Lagrangian,

$$\mathcal{L} = c_0 \int_0^{\bar{L}} d\bar{x} (\cos \theta - 1) \partial_t \varphi - c_1 \mathcal{V}, \quad (34)$$

with the coefficients

$$c_0 = \hbar S \frac{\kappa}{m}, \quad c_1 = JS^2 \frac{m}{\kappa}. \quad (35)$$

We expand φ and θ in the form,

$$\begin{cases} \varphi(\bar{x}, t) = \varphi_0(\bar{x} - \bar{X}(t)) + \sum_{\alpha \neq 0}^\infty \eta_\alpha(t) v_\alpha(\bar{x} - \bar{X}(t)), \\ \theta(\bar{x}, t) = \pi/2 + \sum_{\alpha \neq 0}^\infty \xi_\alpha(t) u_\alpha(\bar{x} - \bar{X}(t)). \end{cases} \quad (36)$$

In the expansion of the θ -mode, it is not necessary to exclude $\alpha = 0$, since the θ -mode does not contain zero mode. This description amounts to using the curvilinear basis, $\{X, \eta_\alpha, \xi_\alpha\}$, in functional space and taking the generalized coordinates,

$$q_1 = \bar{X}, \quad q_{2\alpha} = \eta_\alpha, \quad \text{and} \quad q_{3\alpha} = \xi_\alpha. \quad (37)$$

Since the zero mode $\partial_{\bar{x}} \varphi_0(\bar{x})$ is orthogonal to the phonon modes, we have

$$\int_0^{\bar{L}} d\bar{x} \frac{\partial \varphi_0(\bar{x})}{\partial \bar{x}} v_\alpha(\bar{x}) = 0, \quad (38)$$

for $\alpha \neq 0$. Noting that

$$\dot{\varphi} = -\dot{q}_1 \left(\partial_{\bar{x}} \varphi_0 + \sum_{\alpha} q_{2\alpha} \partial_{\bar{x}} v_\alpha \right) + \sum_{\alpha} \dot{q}_{2\alpha} v_\alpha,$$

and

$$1 - \cos \theta \simeq 1 + \sum_{\alpha} q_{3\alpha} u_\alpha,$$

and plugging these expressions into the Lagrangian (34), we obtain

$$\begin{aligned} \mathcal{L} = -c_0 \left(\sum_{\alpha} \mathcal{J}_\alpha \dot{q}_{2\alpha} - \dot{q}_1 \sum_{\alpha} \mathcal{K}_\alpha q_{3\alpha} \right. \\ \left. + \sum_{\alpha, \beta} \mathcal{M}_{\alpha, \beta} q_{3\alpha} \dot{q}_{2\beta} \right) - c_1 \mathcal{V}, \end{aligned} \quad (39)$$

where higher order terms $\mathcal{O}(q^3)$ are dropped. The overlap coefficients are given by

$$\begin{cases} \mathcal{J}_\alpha = \int_0^{\bar{L}} d\bar{x} v_\alpha(\bar{x}), \\ \mathcal{K}_\alpha = \int_0^{\bar{L}} d\bar{x} \frac{\partial \varphi_0(\bar{x})}{\partial \bar{x}} u_\alpha(\bar{x}), \\ \mathcal{M}_{\alpha\beta} = \int_0^{\bar{L}} d\bar{x} u_\alpha(\bar{x}) v_\beta(\bar{x}). \end{cases} \quad (41)$$

The Lagrangian (39) is *singular* because it does not contain any term of the form $\dot{q}_i \dot{q}_j$, and the rank of the

Hessian matrix ($\partial^2 \mathcal{L} / \partial \dot{q}_i \partial \dot{q}_j$) becomes zero. This means that there is no primary expressible velocities. Therefore we need to construct the Hamiltonian by using the Dirac's algorithm for the constrained Hamiltonian systems. The canonical momenta conjugate to the coordinates $\bar{X}(t)$, $\eta_\alpha(t)$, and $\xi_\alpha(t)$ are given by

$$\begin{cases} p_1 = \partial \mathcal{L} / \partial \dot{q}_1 = c_0 \sum_\alpha \mathcal{K}_\alpha q_{3\alpha}, \\ p_{2\alpha} = \partial \mathcal{L} / \partial \dot{q}_{2\alpha} = -c_0 \left(\mathcal{J}_\alpha + \sum_\beta \mathcal{M}_{\alpha\beta} q_{3\beta} \right), \\ p_{3\alpha} = \partial \mathcal{L} / \partial \dot{q}_{3\alpha} = 0, \end{cases} \quad (42)$$

and we obtain a canonical Hamiltonian,

$$H_c = p_1 \dot{q}_1 + \sum_\alpha p_{2\alpha} \dot{q}_{2\alpha} + \sum_\alpha p_{3\alpha} \dot{q}_{3\alpha} - \mathcal{L}. \quad (43)$$

The Lagrangian (39) itself gives rise to a set of primary constraints,

$$\begin{cases} \phi_1^{(1)} = p_1 - c_0 \sum_\alpha \mathcal{K}_\alpha q_{3\alpha} \approx 0, \\ \phi_{2\alpha}^{(1)} = p_{2\alpha} + c_0 \left(\mathcal{J}_\alpha + \sum_\beta \mathcal{M}_{\alpha\beta} q_{3\beta} \right) \approx 0, \\ \phi_{3\alpha}^{(1)} = p_{3\alpha} \approx 0, \end{cases} \quad (44)$$

where the symbol ≈ 0 means "weakly zero," i.e. $\phi_i^{(1)}$ may have nonvanishing canonical Poisson brackets with some canonical variables. Because of a lack of primary expressible velocities the Hamiltonian with the imposed constraints,

$$H^* = \phi_1^{(1)} \dot{q}_1 + \sum_\alpha \phi_{2\alpha}^{(1)} \dot{q}_{2\alpha} + \sum_\alpha \phi_{3\alpha}^{(1)} \dot{q}_{3\alpha} + c_1 \mathcal{V}, \quad (45)$$

coincides with H_c , i.e. \dot{q}_1 , $\dot{q}_{2\alpha}$, and $\dot{q}_{3\alpha}$ (primary inexpressible velocities) play the role of Lagrangian multipliers. Now, the Hamiltonian H^* governs the equations of motion of the constrained system. The relevant non-zero Poisson brackets are computed as,

$$\left. \begin{cases} \left\{ \phi_1^{(1)}, \phi_{3\alpha}^{(1)} \right\} = -c_0 \mathcal{K}_\alpha, \\ \left\{ \phi_{2\alpha}^{(1)}, \phi_{3\alpha}^{(1)} \right\} = c_0 \sum_\beta \mathcal{M}_{\alpha\beta}, \\ \left\{ \phi_{2\alpha}^{(1)}, \mathcal{V} \right\} = -2c_1 \rho_\alpha q_{2\alpha}, \\ \left\{ \phi_{3\alpha}^{(1)}, \mathcal{V} \right\} = -2c_1 \lambda_\alpha q_{3\alpha}, \end{cases} \right\} \quad (46)$$

and $\{q_i, p_j\} = \delta_{ij}$ gives rise to the constraint conditions, $\dot{\phi}_1^{(1)} = \left\{ \phi_1^{(1)}, H^* \right\} = 0$, $\dot{\phi}_{2\alpha}^{(1)} = \left\{ \phi_{2\alpha}^{(1)}, H^* \right\} = 0$, and $\dot{\phi}_{3\alpha}^{(1)} = \left\{ \phi_{3\alpha}^{(1)}, H^* \right\} = 0$, or in the explicit form

$$\dot{\phi}_1^{(1)} = c_0 \sum_\alpha \mathcal{K}_\alpha \dot{q}_{3\alpha} = 0, \quad (47a)$$

$$\dot{\phi}_{2\alpha}^{(1)} = c_0 \sum_\beta \mathcal{M}_{\alpha\beta} \dot{q}_{3\beta} - 2c_1 \rho_\alpha q_{2\alpha} = 0, \quad (47b)$$

$$\begin{aligned} \dot{\phi}_{3\alpha}^{(1)} &= c_0 \left(\mathcal{K}_\alpha \dot{q}_1 - \sum_\beta \mathcal{M}_{\alpha\beta} \dot{q}_{2\alpha} \right) - 2c_1 \lambda_\alpha q_{3\alpha} \\ &= 0. \end{aligned} \quad (47c)$$

Eq. (47a) gives $\dot{q}_{3\alpha} = 0$ and then Eq. (47b) gives $q_{2\alpha} = 0$. Now, there arises the secondary constraints $\phi_\alpha^{(2)} = q_{2\alpha} \approx 0$ to be constant in time, $\dot{\phi}_\alpha^{(2)} = \left\{ \phi_\alpha^{(2)}, H^* \right\} = \dot{q}_{2\alpha} = 0$, and the consistency condition is fulfilled.

Finally Eq. (47c) relates $q_{3\alpha} = \xi_\alpha$ to $\dot{q}_1 = \dot{X}$, i.e.

$$\xi_\alpha = \frac{c_0}{2c_1} \frac{\mathcal{K}_\alpha}{\lambda_\alpha} \dot{X}. \quad (48)$$

This result has crucial significance in that *there appears finite amplitude of the ϑ -mode*,

$$u(\bar{x}) = \sum_\alpha \xi_\alpha u_\alpha(\bar{x}), \quad (49)$$

only when the collective velocity \dot{X} is finite. This is exactly the manifestation of the ODLRO. In other words, the $u(\bar{x})$ -field is interpreted as the *demagnetization field* that drives the inertial motion of the kink. Using Eq.(48), we reach the final form of the physical Hamiltonian,

$$H_{\text{ph}} = c_1 \sum_\alpha \lambda_\alpha \xi_\alpha^2 = \frac{c_0^2}{4c_1} \sum_\alpha \frac{\mathcal{K}_\alpha^2}{\lambda_\alpha} \dot{X}^2 = \frac{1}{2} M \dot{X}^2, \quad (50)$$

where the inertial mass of the kink crystal is introduced

$$M = \frac{c_0^2}{2c_1} \left(\frac{m}{\kappa} \right)^2 \sum_\alpha \frac{\mathcal{K}_\alpha^2}{\lambda_\alpha}. \quad (51)$$

The physical Hamiltonian (50) describes the inertial motion of the kink crystal.

VI. TRANSPORT MAGNETIC CURRENT

Now we are ready to define the longitudinal spin current. We start with the linear momentum per unit area carried by the kink crystal,

$$P = \hbar S \int_0^{\bar{L}} (1 - \cos \theta) \partial_{\bar{x}} \varphi_0 d\bar{x}. \quad (52)$$

By expanding $\theta = \pi/2 + u$ and $\varphi = \varphi_0$, for a steady current, we obtain

$$\begin{aligned} P &\simeq \hbar S [\varphi_0(\bar{L}) - \varphi_0(0)] + \hbar S \int_0^{\bar{L}} u(\bar{x}) \partial_{\bar{x}} \varphi_0 d\bar{x} \\ &= 2\pi \hbar S \mathcal{Q} + \hbar S \sum_\alpha \xi_\alpha \mathcal{K}_\alpha. \end{aligned} \quad (53)$$

We here introduced the topological charge,

$$\mathcal{Q} = \frac{1}{2\pi} [\varphi_0(\bar{L}) - \varphi_0(0)]. \quad (54)$$

Using Eq.(48), we obtain an important formula,

$$P = 2\pi \hbar S \mathcal{Q} + M \dot{X},$$

that plays an essential role in this paper. The first term is associated with the equilibrium background momentum and the second one corresponds to the transport current carried by the θ -fluctuations. Apparently, the transverse magnetic field increases a period of the kink crystal lattice and diminishes the topological charge \mathcal{Q} and therefore it affects only the *background linear momentum* (see discussion in Sec. X). The physical momentum related with a mass transport due to the excitations around the kink crystal state is generated by the steady movement.

The “superfluid mass current” is accompanied by the “superfluid magnetic current” transferred by the θ -fluctuations. It is determined through the definition of the accumulated magnon density¹⁴ ρ_s in the total magnon density $\mathcal{N} = g\mu_B S(1 - \cos\theta) = \rho_0 + \rho_s$, where the superfluid part is

$$\rho_s = -g\mu_B S \cos\theta. \quad (55)$$

By using $\theta = \pi/2 + u(\bar{x}, t)$, we have

$$\rho_s \simeq g\mu_B S u = g\mu_B S \sum_{\alpha} \xi_{\alpha} u_{\alpha}(\bar{x} - \bar{X}(t)),$$

therefore, for a steady current, we obtain the continuity equation

$$\frac{\partial \rho_s}{\partial t} = -g\mu_B S \frac{c_0}{2c_1} \dot{X}^2 \frac{\partial}{\partial \bar{x}} \left\{ \sum_{\alpha} \frac{\mathcal{K}_{\alpha}}{\lambda_{\alpha}} u_{\alpha}(\bar{x}) \right\} = -\frac{\partial j^x}{\partial \bar{x}}, \quad (56)$$

where we introduced the magnon time-even current carried by the θ -fluctuations

$$j^x(\bar{x}) = g\mu_B S \frac{c_0}{2c_1} \frac{m}{\kappa} \dot{X}^2 \sum_{\alpha} \frac{\mathcal{K}_{\alpha}}{\lambda_{\alpha}} u_{\alpha}(\bar{x}). \quad (57)$$

Here we used the fact $\dot{\xi}_{\alpha} = 0$ because of the constraint. The time evenness is manifested by appearance of not \dot{X} but \dot{X}^2 . The important point to note is that *the only massive θ -mode can carry the longitudinal magnon current as a manifestation of ordering in non-equilibrium state, i.e., dynamical off-diagonal long range order.*

The net magnetization (magnetic dipole moment) induced by the movement is

$$\begin{aligned} m(\bar{x}) &\simeq -g\mu_B S u(\bar{x}) \\ &= -g\mu_B S \frac{c_0}{2c_1} \frac{m}{\kappa} \dot{X} \sum_{\alpha} \frac{\mathcal{K}_{\alpha}}{\lambda_{\alpha}} u_{\alpha}(\bar{x}). \end{aligned} \quad (58)$$

The sign minus means that the net magnetization produces a demagnetization field.

VII. QUANTITATIVE ESTIMATES

To compute the mass M , the spin current j^x and the magnetic dipole moment m , we consider an array of parallel chains described by the model (1), where a number

of chains *per unit area* is $n_{\text{area}} = 1/a_0^2$. In the case of the molecular-based chiral magnets, the crystal packing is usually loose ($a_0 \simeq 10^{-9}$ [m]) and the exchange interaction is rather weak ($J \simeq 10$ [K] $\simeq 10^{-22}$ [J]). On the other hand, in the case of the inorganic chiral magnets, the crystal packing is close ($a_0 \simeq 10^{-10}$ [m]) and the exchange interaction is rather strong ($J \simeq 100$ [K] $\simeq 10^{-21}$ [J]). We take these values as just typical parameter choices. The strength of the Dzyaloshinskii interaction is ambiguous and we simply take $q_0 = D/J = 10^{-2}$.

A. Mass of the kink crystal

The mass M of the kink crystal is given by Eq.(51). Evaluation of the overlap integral \mathcal{K}_{α} is performed in appendix C and yields $\mathcal{K}_{\alpha} = \delta_{\alpha,0} \mathcal{K}_0$, where

$$\mathcal{K}_0 = 2\sqrt{\frac{E(\kappa)}{K(\kappa)} \frac{m}{\kappa} \frac{L}{a_0}}. \quad (59)$$

Therefore we have

$$M = \frac{c_0^2}{2c_1} \left(\frac{m}{\kappa}\right)^2 \frac{\mathcal{K}_0^2}{\lambda_0} \frac{1}{a_0^2}. \quad (60)$$

The factor $1/a_0^2$ appears here after the MKS units [m] for distances are recovered in Eq.(50). The mass per unit area is given by

$$M_{\text{area}} = n_{\text{area}} \times M = \frac{c_0^2}{2c_1} \left(\frac{m}{\kappa}\right)^2 \frac{\mathcal{K}_0^2}{\lambda_0} \frac{1}{a_0^4}, \quad (61)$$

that after simplification yields

$$M_{\text{area}} = \frac{2E(\kappa)}{\lambda_0 K(\kappa)} \frac{\hbar^2 L}{J a_0^5} \simeq \frac{\hbar^2 L}{J a_0^5}.$$

The last relationship is reliable in the case of small fields, i.e. $\lambda_0 \simeq 2$, and $K(\kappa) = E(\kappa) \simeq \pi/2$.

Noting that the period of kink measured in lattice units is given by Eq.(7), which turns into $\ell_{\text{kink}} = 8K(\kappa)E(\kappa)/\pi q_0 \simeq 2\pi J/D$ for small fields, the mass per one kink acquires the form

$$M_{\text{kink}} = M_{\text{area}} \frac{\ell_{\text{kink}}}{L} \simeq \frac{J}{D} \frac{\hbar^2}{J a_0^4}. \quad (62)$$

As a typical example of the molecular-based chiral magnets, we have

$$M_{\text{kink}} \simeq 10^{-9} [\text{g}/\text{cm}^2].$$

For the chain length $L/a_0 = 10^5$, we have the total mass $M_{\text{area}} \simeq \frac{D}{J} \frac{L}{a_0} M_{\text{kink}} \simeq 10^{-4} [\text{g}/\text{cm}^2]$. As a typical example of the inorganic chiral magnets, we have

$$M_{\text{kink}} \simeq 10^{-6} [\text{g}/\text{cm}^2].$$

For the chain length $L/a_0 = 10^6$, we have the total mass $M_{\text{area}} \simeq 10^{-2} [\text{g}/\text{cm}^2]$. This heavy mass should be compared with the mass of conventional Bloch wall mass in

ferromagnets. To make clear the difference, in appendix D, we gave a brief summary of this issue. In the present case, appearance of the heavy mass is easily understood, since the kink crystal consists of a macroscopic array of large numbers of local kinks.

B. Spin current

As it follows from the continuity equation (56) the physical dimension of the spin current density is $\text{Wb} \cdot \text{m}^2/\text{s}$. Using the results of the appendix C the spin current density given by Eq.(57) transforms into

$$j^x(\bar{x}) = g\mu_B S \frac{c_0}{2c_1} \frac{m}{\kappa} \frac{1}{a_0} \dot{X}^2 \frac{\mathcal{K}_0}{\lambda_0} u_0(\bar{x}). \quad (63)$$

The factor $1/a_0$ occurs after the MKS units for distances are recovered in the continuity equation $\partial_x \rightarrow a_0 \partial_x$ and in the velocity $\dot{X} \rightarrow \dot{X}/a_0$. After simplifications with aid of Eqs.(6), (35), (30), and (59) we immediately have

$$j^x(\bar{x}) = \frac{g\mu_B \hbar}{J a_0} \frac{4E(\kappa)}{\pi q_0} \frac{1}{\lambda_0} \dot{X}^2 \text{dn}(\bar{x}, \kappa). \quad (64)$$

For the case of weak fields corresponding to small κ this yields

$$j^x(\bar{x}) \simeq \frac{g\mu_B \hbar}{J a_0 q_0} \dot{X}^2 \text{dn}(\bar{x}, \kappa). \quad (65)$$

We present a schematic view of an instant distribution of spins in the current-carrying state in Fig. 6. In Fig. 7, we present a snapshot of the position dependence of the current density $j^x(x)$ in the weak field limit, given by Eq. (65). In Fig. 7, we depicted the cases of the magnetic field strengths $\tilde{H}/\tilde{H}_c = 0.1, 0.5$, and $\tilde{H}/\tilde{H}_c \simeq 1$. Although the formula (65) is valid only for the case of weak field limit, but qualitative features are well demonstrated by just extrapolating the validity up to $\tilde{H}/\tilde{H}_c \simeq 1$. As the field strength approaches the critical value, the current density is more and more localized.

For both the typical molecular-based and inorganic chiral magnets, we have

$$j^x(\bar{x}) \sim 0.1 \mu_B \dot{X}^2 \sim 10^{-24} \dot{X}^2 [\text{Wb} \cdot \text{s}].$$

Taking the velocity of order $\dot{X} \sim 10^2$ [m/s] we obtain finally

$$j^x(\bar{x}) \sim 10^{-20} [\text{Wb} \cdot \text{m}^2/\text{s}],$$

therefore the current through the unit area

$$j_{\text{area}}^x(\bar{x}) = j^x(\bar{x}) \times n_{\text{area}} \sim 1 [\text{Wb}/\text{s}].$$

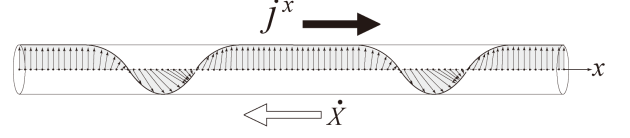


FIG. 6: A schematic view of an instant distribution of spins in the current-carrying state. This picture corresponds to the case of intermediate field strength.

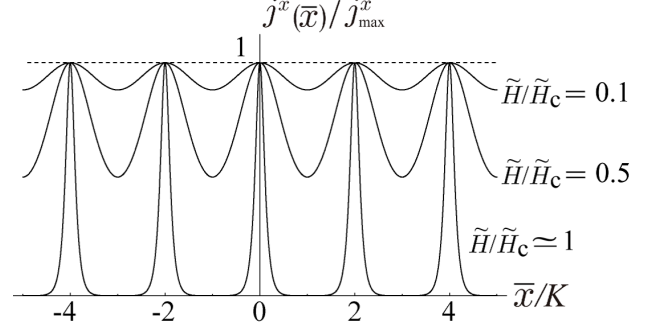


FIG. 7: A snapshot of the position dependence of the current density $j^x(\bar{x})$. $j^x(\bar{x})$ is scaled by its maximum $j_{\text{max}}^x = j^x(0)$. We depicted the cases of the magnetic field strengths $\tilde{H}/\tilde{H}_c = 0.1, 0.5$, and $\tilde{H}/\tilde{H}_c \simeq 1$.

C. Magnetic dipole moment

The magnetic dipole moment [Eq.(58)] induced by the motion is given by

$$m(\bar{x}) = -g\mu_B S \frac{c_0}{2c_1} \frac{m}{\kappa} \frac{1}{a_0} \dot{X} \frac{\mathcal{K}_0}{\lambda_0} u_0(\bar{x}),$$

i.e. the relationship $j^x = -m \dot{X}$ holds. By the same manner as it was made for the spin current we obtain in the case of the small fields

$$m(\bar{x}) \simeq -\frac{g\mu_B \hbar}{J a_0 q_0} \dot{X} \text{dn}(\bar{x}, \kappa). \quad (66)$$

Therefore, for both the molecular-based and inorganic chiral magnets, we have

$$m(\bar{x}) \sim 0.1 \mu_B \dot{X} \sim 10 \mu_B, \quad (67)$$

i.e. $m(\bar{x})$ is of order 10^{-22} [Wb · m]. The total magnetic moment of the chain is

$$\begin{aligned} m_{\text{chain}} &\simeq -\frac{g\mu_B \hbar}{J a_0 q_0} \dot{X} \int_0^L \text{dn}(\bar{x}, \kappa) d\bar{x} \\ &= -\frac{g\mu_B \hbar}{J a_0 q_0} \pi \mathcal{Q} \dot{X}. \end{aligned} \quad (68)$$

We here used the relations $\int \text{dn}(\bar{x}, \kappa) d\bar{x} = \text{am}(\bar{x}, \kappa)$ and $[\varphi_0(x) + \pi]/2 = \sin^{-1}[\text{sn}(\bar{x}, \kappa)] = \text{am}(\bar{x}, \kappa)$ that

leads to

$$\int_0^{\bar{L}} \text{dn}(\bar{x}, \kappa) d\bar{x} = \frac{1}{2} [\varphi_0(\bar{L}) - \varphi_0(0)] = \pi \mathcal{Q}, \quad (69)$$

where \mathcal{Q} is a topological charge introduced in Eq.(54).

Noting,

$$\mathcal{Q} = L/l_{\text{kink}} = \frac{\pi q_0 L}{8K(\kappa)E(\kappa)a_0}, \quad (70)$$

we have the chain magnetization

$$m_{\text{chain}} \simeq -\frac{g\mu_B \hbar}{2Ja_0} \left(\frac{L}{a_0}\right) \dot{X}.$$

The total moment per unit volume

$$m_{\text{vol}} = m_{\text{chain}} \times n_{\text{area}} \times L^2 \simeq -\frac{g\mu_B \hbar}{2Ja_0} \left(\frac{L}{a_0}\right)^3 \dot{X}.$$

As a typical example of the molecular-based chiral magnets, we have

$$m_{\text{vol}} \sim 10^{-11} \dot{X} \sim 10^{-9} [\text{Wb} \cdot \text{m}].$$

As a typical example of the inorganic chiral magnets, we have

$$m_{\text{vol}} \sim 10^{-8} \dot{X} \sim 10^{-6} [\text{Wb} \cdot \text{m}].$$

VIII. DISCUSSIONS OF RELATED TOPICS

A. Background spin current problem: SU(2) gauge invariant formulation

Heurich, König and MacDonald³⁷ proposed that the external magnetic fields generate dissipationless spin currents in the ground state of systems with spiral magnetic order. Here, we comment on the relevance of the present work to this issue. In our model, the *background* spin current is given by

$$j_{\text{bg}} = \partial\varphi_0(\bar{x})/\partial\bar{x} - \bar{q}_0 \propto \text{dn}(\bar{x}) - 2E(\kappa)/\pi, \quad (71)$$

i.e. there arises the misfit of the kink crystal to the helimagnetic modulation and consequently the current comes up. Below we prove that this current exists on a link between two sites but it causes no accumulation of magnon density ("magnetic charge") at the site due to continuity equation, i.e. the current is not related to the magnon transport. This supports reasonings of arguments by Schütz, Kopietz, and M. Kollar³⁹ that appearance of finite spin currents is direct manifestation of quantum correlations in the system, and in the classical ground state the spin currents vanish.

The background spin current problem is best described by the SU(2) gauge invariant formulation developed by

Chandra, Coleman and Larkin.³⁸ By imposing the local SU(2) gauge invariance of the theory, we obtain the fictitious SU(2) gauge fields \mathbf{a} and \mathbf{h} that give the spin current $\mathbf{J}^{(S)} = \partial\mathcal{L}_g/\partial\mathbf{a}$, and the spin density $\mathbf{S} = \partial\mathcal{L}_g/\partial\mathbf{h}$, respectively, where \mathcal{L}_g is the gauge-invariant Lagrangian.

Following Chandra, Coleman and Larkin, we use the SU(2) Schwinger boson representation,

$$\mathbf{S}_i = \frac{1}{2} b_{i\alpha}^\dagger \sigma_{\alpha\beta} b_{i\beta}, \quad \sum_{\alpha} b_{i\alpha}^\dagger b_{i\alpha} = 2S, \quad (\alpha = 1, 2) \quad (72)$$

where $\sigma = (\sigma_x, \sigma_y, \sigma_z)$ are the Pauli matrices. In the path-integral prescription, the partition function is represented as

$$\mathcal{Z} = \int \mathcal{D}b_{i\alpha}^\dagger \mathcal{D}b_{i\alpha} \mathcal{D}\lambda_i \exp\left(-\int_0^\beta \mathcal{L}(\tau) d\tau\right), \quad (73)$$

where the Lagrangian is given by

$$\begin{aligned} \mathcal{L}(\tau) = & \sum_i \left[b_{i\alpha}^\dagger \partial_\tau b_{i\alpha} + i\lambda_i (b_{i\alpha}^\dagger b_{i\alpha} - 2S) \right] \\ & + \mathcal{H}[S(b^\dagger, b)], \end{aligned} \quad (74)$$

where \mathcal{H} is the Hamiltonian (1) written in terms of the Schwinger bosons, and τ represents the imaginary time. The Lagrange multiplier λ_i provides the local constraint. The local SU(2) gauge transformation acting on the SU(2) doublet, $b_i^+ = (b_{i1}^+, b_{i2}^+)$ is given by

$$b_i'^+ = b_i^+ \hat{g}_i^{-1}, \quad b'_i = \hat{g}_i b_i, \quad (75)$$

where

$$\hat{g}_i(t) = \exp\left[-\frac{i}{2} \boldsymbol{\Theta}_i(t) \cdot \boldsymbol{\sigma}\right]. \quad (76)$$

The SU(2) rotation \hat{g}_i gives the rotation of the spin vector,

$$\mathbf{S}'_i = \exp\left(-\boldsymbol{\Theta}_i \cdot \hat{\mathbf{I}}\right) \mathbf{S}_i \simeq \mathbf{S}_i - \boldsymbol{\Theta}_i \times \mathbf{S}_i, \quad (77)$$

where $(\hat{I}_\mu)_{\nu\lambda} = \varepsilon_{\mu\nu\lambda}$ ($\mu, \nu, \lambda = x, y, z$) is the adjoint representation of the Lie algebra of the SO(3) group characterized by $[\hat{I}_\mu, \hat{I}_\nu] = \varepsilon_{\mu\nu\lambda} \hat{I}_\lambda$.

Rewriting the Lagrangian in the gauge invariant form, there appears a term

$$b_{i\alpha}^\dagger (\hat{g}_i \partial_\tau \hat{g}_i^{-1}) b'_{i\alpha} = i e^{\boldsymbol{\Theta}_i \cdot \hat{\mathbf{I}}} \partial_\tau \boldsymbol{\Theta}_i \cdot \mathbf{S}'_i, \quad (78)$$

that leads to introducing the gauge field \mathbf{h}_i transformed as

$$\mathbf{h}_i \rightarrow \mathbf{h}'_i = e^{\boldsymbol{\Theta}_i \cdot \mathbf{I}} (\mathbf{h}_i + \partial_t \boldsymbol{\Theta}_i), \quad (79)$$

where $\tau = it$. Introducing the gauge covariant time derivative, $\mathcal{D}_t \equiv \partial_t - \mathbf{h} \times$, we have $\mathbf{h}'_i = \mathbf{h}_i + \mathcal{D}_t \boldsymbol{\Theta}_i$. The

fictitious magnetic field $\nabla_t \Theta_i$ is induced by the time-dependent rotation of the spin reference frame.

The exchange terms are regrouped in a gauge-invariant form,

$$\begin{aligned} & -J \sum_{\langle i,j \rangle} \mathbf{S}_i \cdot \mathbf{S}_j + \mathbf{D} \cdot \sum_{\langle i,j \rangle} \mathbf{S}_i \times \mathbf{S}_j \\ & = -\mathcal{J} \sum_{\langle i,j \rangle} \mathbf{S}_j \exp \left[- \left(\int_{x_i}^{x_j} \mathbf{a} \cdot d\mathbf{r} \right) \hat{I}_x \right] \mathbf{S}_i, \end{aligned} \quad (80)$$

where $\mathcal{J} = \sqrt{J^2 + D^2}$, where x_i represents the position of the i -th site, and the spin vector potential is introduced as $a_x = (D/J) \hat{e}_x$, $a_y = a_z = 0$, corresponding to the model

(1). The form of Eq.(80) indicates that the tangential phase angle φ_i can be gauged away by the local rotation of the angle $(D/J) R_{xi}$ around the x axis. The gauge field \mathbf{a} is transformed as

$$\mathbf{a}_i \rightarrow \mathbf{a}'_i = e^{\Theta_i \mathbf{I}} (\mathbf{a} - \partial_{x_i} \Theta_i), \quad (81)$$

or $\mathbf{a}'_i = \mathbf{a} - \nabla_{x_i} \Theta_i$ via the gauge covariant space derivative $\nabla_{x_i} \equiv \partial_{x_i} + \mathbf{a} \times$. In addition to the physical gauge field, $(D/J) \hat{e}_x$, there appears the fictitious gauge field, $\nabla_{x_i} \Theta_i$, induced by the spatial rotation of the spin reference frame.

The variation of the partition function under a local gauge transformation must be zero

$$\delta \mathcal{Z} = \int \mathcal{D}b_{i\alpha}^\dagger \mathcal{D}b_{i\alpha} \mathcal{D}\tilde{\lambda}_i \exp \left(- \int \mathcal{L}_g(\tau) d\tau \right) \left(\frac{\partial \mathcal{L}_g}{\partial \mathbf{a}'_i} \cdot \delta \mathbf{a}'_i + \frac{\partial \mathcal{L}_g}{\partial \mathbf{h}'_i} \cdot \delta \mathbf{h}'_i \right) = 0, \quad (82)$$

where $\delta \mathbf{a}'_{i\alpha} = -\nabla_{x_i} \delta \Theta_i$, $\delta \mathbf{h}'_i = \nabla_t \delta \Theta_i$. Consequently, one obtains the conservation law

$$\nabla_{x_i} (\partial \mathcal{L}_g / \partial \mathbf{a}'_i) - \nabla_t (\partial \mathcal{L}_g / \partial \mathbf{h}'_i) = 0. \quad (83)$$

By definition $(\partial \mathcal{L}_g / \partial \mathbf{a}'_i)|_{\mathbf{a}'_i = \mathbf{a}} = \mathbf{J}_i^{(S)}$ is the spin current, where the gauge field is fixed by the Dzyaloshinskii vector. On the other hand $\partial \mathcal{L}_g / \partial \mathbf{h}'_i = -\mathbf{h}_i$, and we finally obtain the continuity equation

$$\nabla_{x_i} \mathbf{J}_i^{(S)} + \nabla_t \mathbf{S}_i = 0, \quad (84)$$

where $\mathbf{J}_i^{(S)} = \mathbf{J}_{i \rightarrow i+1}^{(S)} + \mathbf{J}_{i-1 \rightarrow i}^{(S)}$. In the explicit form, the spin current from the site i to $i+1$ is given by

$$\begin{aligned} \mathbf{J}_{i \rightarrow i+1}^{(S)} & = J x_i (\mathbf{S}_i \times \mathbf{S}_{i+1}) + x_i [(\mathbf{D} \times \mathbf{S}_{i+1}) \times \mathbf{S}_i] \\ & = S^2 \mathcal{J} \sin(\varphi_{i+1} - \varphi_i - \varphi_0) \hat{e}_x, \end{aligned}$$

where x_i represents the position of the i -th site.

For the long-period incommensurate structure ($D/J \leq 1$) this yields in the continuum limit

$$\mathbf{J}_{i \rightarrow i+1}^{(S)} \simeq JS^2 \left(\frac{\partial \varphi}{\partial x} - \frac{D}{J} \right) \hat{e}_x. \quad (85)$$

The spin current from the site $i-1$ to the site i

$$\mathbf{J}_{i-1 \rightarrow i}^{(S)} = J x_i (\mathbf{S}_i \times \mathbf{S}_{i-1}) - x_i [(\mathbf{D} \times \mathbf{S}_i) \times \mathbf{S}_{i-1}]$$

gives $-\mathbf{J}_{i \rightarrow i+1}^{(S)}$ in the continuum limit and compensates (85). Thus, the spin current through the i -th site causes no accumulation of magnon density at the site, i.e. *the current is not transport one*. The accumulation of magnon density means that the local quantization axis is wobbling. This wobbling motion, however, contradicts the spontaneous symmetry breaking in the *ground state*.

B. Spin supercurrent in ^3He

The moving kink crystal belongs to a class of dynamical systems out of equilibrium.¹⁴ In contrast to a class of equilibrium macroscopic ordered state with a broken symmetry (ordered magnets, liquid crystals, superfluids and superconductors) an emerging steady state is supported by pumping of energy. The coherent spin precession discovered in superfluid ^3He known as homogeneously precessing domains (HPD) is a striking example of the quantum state.

The precession of magnetization (spin) occurs after the magnetization is deflected by a finite angle by the rf field from its equilibrium value. The Larmor precession spontaneously acquires a coherent phase throughout the whole sample. This is equivalent to the appearance of a coherent superfluid Bose condensate, i.e. HPD is the Bose-condensate of magnons. According to the analogy the deviation of the spin projection from its equilibrium value in the precession plays the role of the number density of magnons. In terms of magnon condensation the precession can be viewed as the off-diagonal long-range order for magnons, where the phase of precession plays the role of the phase of the superfluid order parameter, and the precession frequency plays the role of chemical potential.

The remarkable property of the magnon Bose condensate in $^3\text{He-B}$ is that non-equilibrium precession has a fixed density of Bose condensate. The density cannot relax continuously, a decay of the condensate occurs due to decreasing volume of the superfluid part. This results in the formation of two regions of precession: the domain with HPD is separated by a phase boundary, where a precession frequency equals to the Larmor frequency,

from the domain with static equilibrium magnetization (non-precessing domain, NPD). In the absence of a continuous pumping, i.e. rf field, HPD remains in the fully coherent Bose condensate state, while the phase boundary between HPD and NPD slowly moves up to decrease a volume of the Bose condensate.

We may suggest that in the total analogy with the supercurrents in ^3He , i.e. spin currents transferred by the coherent spin precession, the pumping of magnons in the kink crystal (by ultrasound, for example) will cause an appearance of homogeneously moving domains with ODLRO separated by a phase boundary from the domain with a static soliton lattice. Without an external flux of energy, the relaxation will occur via gradual decrease of the volume of the superfluid phase.

C. Experimental aspects

In realizing the bulk magnetic current proposed here, a single crystal of chiral magnets serves as spintronics device. The mechanism involves no spin-orbit coupling and the effect is not hindered by dephasing. Finally, we propose possible experimental methods to trigger off the spin current considered here.

1. Spin torque mechanism and spin current amplification

The spin-polarized electric current can exert torque to ferromagnetic moments through direct transfer of spin angular momentum.² This effect, related with Aharonov-Stern effect⁷ for a classical motion of magnetic moment in an inhomogeneous magnetic field, is eligible to excite the sliding motion of the kink crystal by injecting the spin-polarized current (polarized electron beam) in the direction either perpendicular or oblique to the chiral axis. The spin current transported by the soliton lattice may amplify the spin current of the injected carriers.

2. XMCD

To detect the magnetic dipole moment dynamically induced by the kink crystal motion, x-ray magnetic circular dichroism (XMCD) may be used. Photon angular momentum may be aligned either parallel or anti-parallel to the direction of the longitudinal net magnetization.

3. Ultrasound attenuation under the magnetic field

Further possibility to control and detect the spin current is using a coupling between spins and chiral torsion. Fedorov *et al*⁴¹ first pointed out that under the external torsion, the magneto-elastic coupling of the form, $\sum_{\mathbf{R}_i, \mathbf{R}_j} g_{ij} [\nabla \times (\mathbf{u}_i - \mathbf{u}_j)] \cdot \mathbf{S}_i \times \mathbf{S}_j$, appears, where \mathbf{u}_i is the displacement of the magnetic atom at a lattice point

\mathbf{R}_i . Then, the quantity $\mathbf{d}_{ij} = g_{ij} [\nabla \times (\mathbf{u}_i - \mathbf{u}_j)]$ plays a role of an effective Dzyaloshinskii interaction. Ultrasound with the wavelength being adjusted to the period of the kink crystal may resonantly modulate \mathbf{d}_{ij} and may exert the periodic torque on the kink crystal. Consequently, the kinetic energy is supplied to the kink crystal and the ultrasound attenuation may occur.⁴² Then, the attenuation rate should change upon changing the applied magnetic field strength.

4. TOF technique

The most direct way of detecting the traveling magnon density may be winding a sample by a pick-up coil and performing the time-of-flight (TOF) experiment. Then, the coil should detect a periodic signal induced by the magnetic current.

5. Energy loss of the moving kink crystals

The moving kink crystal produces the time-varying vector potential *per kink*,

$$\mathbf{A}(\mathbf{r}, t) = \frac{\mu_0}{4\pi} \frac{\mathbf{m}(x - Vt) \times \mathbf{r}}{r^3}, \quad (86)$$

where $V = \dot{X}$ and \mathbf{r} is the position vector with respect to the kink center. Then, the magnitude of the induced azimuthal electric field \mathbf{E} around the chiral axis is given by

$$E_\varphi(\rho) = \left| \frac{\partial A_\varphi}{\partial t} \right| \simeq \frac{3\mu_0}{4\pi} \frac{g\mu_B\hbar}{Ja_0q_0} V^2 \frac{\rho x}{(x^2 + \rho^2)^{5/2}}, \quad (87)$$

where ρ is the radial coordinate. Then, in the *metallic* chiral magnets, strong energy loss may occur due to the induced eddy currents. This phenomena is exactly analogous to a well known fact that a magnet moving through inside of the metallic pipe feels strong friction. On the other hand, in the *insulating* chiral magnets, there is no eddy current loss and instead the polariton excitations are expected to occur. Therefore, the frictional force acting on the moving crystal can be strongly diminished in the insulating magnets.⁴³

IX. CONCLUDING REMARKS

In this paper, we gave a detailed account of a mechanism of possible longitudinal transport spin current in the chiral helimagnet under transverse magnetic field. The most important notion is that the "spin phase" directly comes up in the observable effects through the soliton lattice formation. In our mechanism, the current is carried by the moving magnetic kink crystal, where the linear momentum has a form, $P = 2\pi SQ + M\dot{X}$. The topological magnetic charge, SQ , merely enters the equilibrium

background momentum $2\pi S\mathcal{Q}$, while the collective translation of the kinks with the velocity \dot{X} gives the mass M . We examined the Gaussian fluctuations around the kink crystal state in the soliton sector and showed that the longitudinal θ fluctuations (along with the helical axis) plays a crucial role to determine the mass of kinks. Appearance of the spin currents is a manifestation of ordering in non-equilibrium state, i.e., dynamical off-diagonal long range order.

We also stressed that if we took account of only the φ -fluctuations, the spin current (Josephson current) would cause no accumulation of magnon density and the current is not transport one. The accumulation of magnon density means that the local quantization axis is wobbling but this contradicts the spontaneous symmetry breaking in the ground state.

This mechanism is quite analogous to the Döring-Becker-Kittel mechanism of the domain wall motion, i.e., the Galilean boost of the solitonic kink. In our case, the coherent motion of the kink crystal is dynamically induced by spontaneous emergence of the demagnetization field. To describe the kink crystal motion and resultant emergence of the demagnetization field, we revisited the Sutherland's seminal work³⁰ and generalized it to the case of vectorial degrees of freedom, i.e., not only the tangential φ but and the longitudinal θ degrees of freedom are considered. To clarify the physical meaning of the inertial mass, we developed the canonical formulation of the kink crystal motion. We showed that in the case of molecular-based chiral magnets, the inertial mass per kink amounts to $M_{\text{kink}} \simeq 10^{-9}[\text{g}/\text{cm}^2]$ and the total mass $M_{\text{area}} \simeq 10^{-4}[\text{g}/\text{cm}^2]$. In the case of the inorganic chiral magnets, $M_{\text{kink}} \simeq 10^{-6}[\text{g}/\text{cm}^2]$, and the total mass $M_{\text{area}} \simeq 10^{-2}[\text{g}/\text{cm}^2]$. Furthermore, the magnetic dipole moment per kink, induced by the kink crystal motion, amounts to $m \sim 0.1 \mu_B \dot{X} \sim 10 \mu_B$. Appearance of the heavy mass is a consequence of the fact that the kink crystal consists of a macroscopic array of large numbers of local kinks.

We here mention that in our scheme, the energy gap of the θ -mode plays a role of "protector" of the rigid sliding motion of the kink crystal. To excite the θ -mode, we need to supply the energy via the external force. This situation is reminiscent of the existence of the edge velocity like Larmor frequency in the superfluid ^3He . To make clear the physical nature of the edge velocity in our scheme is beyond the scope of the present work. We leave this problem for future consideration.

Detection of these observable quantities may be quite a promising challenge for experimentalists. Behind this issue, there is an actively argued problems on how to make use of the indirect couplings among the magnetic, electronic, and elastic degrees of freedom. For example, magnetic-field-dependent ultrasonic attenuation may give us a new insights. To materialize the theoretical model presented here, symmetry-adapted material synthesis would be required. So far, a novel category of materials suitable for chiral magnets has been success-

fully fabricated on purpose for application in the field of both molecule-based and inorganic magnetic materials. The interplay of crystallographic and magnetic chirality plays a key role there. The materials of this category are not only of keen scientific interest, but they may also open a possible new window for new device synthesis and fabrication in spintronics.

Acknowledgments

We acknowledge helpful discussions with J. Akimitsu, I. Fomin, K. Inoue, Yu. A. Izyumov, and K. Kikuchi. J. K. acknowledges Grant-in-Aid for Scientific Research (A)(No. 18205023) and (C) (No. 19540371) from the Ministry of Education, Culture, Sports, Science and Technology, Japan.

APPENDIX A: PERIODIC POTENTIAL AND BLOCH THEOREM

We have Schrödinger equation

$$-\frac{d^2u}{d\bar{x}^2} + V(\bar{x})u = \varepsilon u, \quad (\text{A1})$$

where the periodic potential has a period $2K$

$$V(\bar{x} + 2K) = V(\bar{x}) \quad (\text{A2})$$

and given explicitly by

$$V(\bar{x}) = 6\kappa^2 \text{sn}^2(\bar{x}) - \kappa^2 - 4 + 4\bar{q}_0 \text{dn} \bar{x}. \quad (\text{A3})$$

According to Bloch theorem a class of bounded states is given by

$$u(\bar{x}) = e^{iQ\bar{x}} \phi_Q(\bar{x})$$

where $\phi_Q(\bar{x})$ is a periodic function $\phi_Q(\bar{x} + 2K) = \phi_Q(\bar{x})$ and Q is a Floquet index. It may be shown (see Ref.⁴⁴, for example) that boundary points of bands are determined from

$$\cos(2KQ) = \pm 1,$$

that produces boundary points of Brillouin zones

$$Q_{BZ}^{(n)} = \frac{\pi}{2K}n, \quad n = \pm 1, \pm 2, \dots$$

The periodicity condition (A2) means that the potential may be expanded into the Fourier series

$$V(\bar{x}) = \sum_{G_n} V_n e^{iG_n \bar{x}},$$

where the reciprocal lattice points are $G_n = 2\pi n/(2K)$, n is integer.

To find Fourier coefficients of the potential $V(\bar{x})$ we use Fourier series for $\text{dn}(\bar{x})$ and $\text{sn}^2(\bar{x})$ functions

$$\text{dn}(\bar{x}) = \frac{\pi}{2K} + \frac{\pi}{K} \sum_{n=1}^{\infty} \frac{\cos(\pi n \bar{x}/K)}{\cosh(\pi n K'/K)}$$

$$\text{sn}^2(\bar{x}) = \frac{K-E}{K\kappa^2} - \sum_{n=1}^{\infty} \frac{\pi^2 n}{\kappa^2 K^2} \frac{\cos(\pi n \bar{x}/K)}{\sinh(\pi n K'/K)}$$

Plugging these series into (A3) we obtain

$$V_0 = 1 + \kappa'^2 - 6\frac{E}{K} + \frac{2\pi}{K}\bar{q}_0,$$

$$V_n = -\frac{3\pi^2}{K^2} \frac{n}{\sinh(\pi n K'/K)} + \frac{2\pi\bar{q}_0}{K} \frac{1}{\cosh(\pi n K'/K)}.$$

The zeroth-order component V_0 determines a shift and may be omitted while the component V_n mixes the plane waves with wave vectors \tilde{k} and $\tilde{k}' = \tilde{k} + \pi n/K$

$$\langle \tilde{k}' | V(\bar{x}) | \tilde{k} \rangle = \sum_n V_n \delta_{\tilde{k}', \tilde{k} + G_n} = \sum_n V_n \delta_{\tilde{k}', \tilde{k} + \pi n/K}.$$

Hence, a quasidegenerate perturbation theory built in the subspace spanned by two states $|\tilde{k}\rangle$ and $|\tilde{k} + G_n\rangle$

$$\begin{vmatrix} E_k^0 & V_n \\ V_n^* & E_{k+G_n}^0 \end{vmatrix} = 0 \quad (\text{A4})$$

yields bands

$$E_{\pm}(\tilde{k}) = \frac{1}{2} \left(E_k^0 + E_{k+G_n}^0 \right) \pm \sqrt{\frac{\left(E_k^0 - E_{k+G_n}^0 \right)^2}{4} + |V_n|^2}.$$

The gap between the states $|-Q_{BZ}^{(n)}\rangle$ and $|-Q_{BZ}^{(n)} + G_n\rangle$ is

$$2|V_n| = \left| -\frac{6\pi^2}{K^2} \frac{n}{\sinh(\pi n K'/K)} + \frac{4\pi\bar{q}_0}{K} \frac{1}{\cosh(\pi n K'/K)} \right|,$$

and it falls rapidly to zero with increasing of n

$$2|V_n| \simeq \exp(-\pi n K'/K).$$

APPENDIX B: LAMÉ EQUATION

The basic properties of the Lamé equation are presented here. We start with the Jacobi form which is defined by³⁴

$$\frac{d^2 \Lambda_{\bar{\alpha}}(x)}{dx^2} = [\ell(\ell+1)\kappa^2 \text{sn}^2(x, \kappa) - \kappa^2(1+A)] \Lambda_{\bar{\alpha}}(x), \quad (\text{B1})$$

where $\ell = 1$ and A being a constant. The spectrum is labeled by a complex parameter $\bar{\alpha}$ and given by

$$A_{\bar{\alpha}} = \frac{1}{\kappa^2} \text{dn}^2 \bar{\alpha}. \quad (\text{B2})$$

The solution of the Lamé equation is exactly given in the conventional form³⁴

$$\Lambda_{\bar{\alpha}}(x) = \frac{\text{H}(x - \bar{\alpha})}{\Theta(x)} e^{xZ(\bar{\alpha})}, \quad (\text{B3})$$

where H , Θ , and Z are Jacobi's eta, theta, and zeta functions, respectively, with the elliptic modulus κ . Now, we require Eq.(B3) to be a propagating Bloch wave, i.e., $Z(\bar{\alpha})$ to be pure imaginary. Recalling that the zeta function $Z(\bar{\alpha})$ is singly periodic with the period $2K$, we see that two segments $(K - 2iK', K]$ and $[-2iK', 0)$ for $\bar{\alpha}$ are sufficient to fully describe the solution (B3).

Because of the quasi-periodicity,

$$H(x + 2K - \bar{\alpha}) = -H(x - \bar{\alpha}), \quad \Theta(x + 2K) = \Theta(x),$$

we have

$$\Lambda_{\bar{\alpha}}(x + 2K) = -e^{2KZ(\bar{\alpha})} \Lambda_{\bar{\alpha}}(x),$$

and it is convenient to introduce the Floquet index

$$\bar{Q}(\bar{\alpha}) = \frac{\pi}{2K} + iZ(\bar{\alpha}, k).$$

Then, we have

$$\Lambda_{\bar{\alpha}}(x + 2K) = e^{-2K i \bar{Q}} \Lambda_{\bar{\alpha}}(x),$$

that is analogous to the Bloch theorem where $2K$ and \bar{Q} have the meanings of the lattice constant and the quasi-momentum, respectively. Furthermore, imposing the periodic boundary condition

$$\begin{aligned} \Lambda_{\bar{\alpha}}(x + L) &= \Lambda_{\bar{\alpha}}\left(x + \frac{L}{2K} 2K\right) = \left[e^{-2K i \bar{Q}} \right]^{\frac{L}{2K}} \Lambda_{\bar{\alpha}}(x) \\ &= e^{-iL \bar{Q}} \Lambda_{\bar{\alpha}}(x) = \Lambda_{\bar{\alpha}}(x), \end{aligned} \quad (\text{B4})$$

we have the quasi-momentum as usual,

$$\bar{Q} = \frac{2\pi}{L} n, \quad n \text{ is integer.}$$

Finally, we have the Bloch form,

$$\Lambda_{\bar{\alpha}}(x) = \frac{\text{H}(x - \bar{\alpha})}{\Theta(x)} e^{-i\bar{Q}x} e^{i\frac{\pi}{2K}x}.$$

Other than the conventional parameterization, it is convenient to work with a real parameter α related with $\bar{\alpha}$ by

$$\bar{\alpha} = i\alpha + K - iK' \quad (\text{B5})$$

for the acoustic branch, and

$$\bar{\alpha} = i\alpha - iK' \quad (\text{B6})$$

for the optic one. Within the new parametrization the eigenfunction for the acoustic mode transforms in the following way

$$\begin{aligned} & H(x - i\alpha - K + iK') \\ &= \vartheta_1\left(\frac{\pi}{2K}[x - x_0 + iK']\right) \\ &= ie^{\frac{\pi K'}{4K}} e^{i\frac{\pi}{2K}x_0} e^{-i\frac{\pi}{2K}x} \vartheta_4\left(\frac{\pi}{2K}[x - x_0]\right), \end{aligned}$$

where $x_0 = i\alpha + K$. Furthermore, we have

$$\vartheta_3\left(\frac{\pi}{2K}[x_0 - iK']\right) = e^{\frac{\pi K'}{4K}} e^{i\frac{\pi}{2K}x_0} \vartheta_2\left(\frac{\pi}{2K}x_0\right),$$

and

$$H(x - \bar{\alpha}) = i \frac{\vartheta_3\left(\frac{\pi}{2K}[x_0 - iK']\right)}{\vartheta_2\left(\frac{\pi}{2K}x_0\right)} e^{-i\frac{\pi}{2K}x} \vartheta_4\left(\frac{\pi}{2K}[x - x_0]\right),$$

that yields

$$\Lambda_{\bar{\alpha}}(x) = \Lambda_{\alpha}(x) = i \frac{\vartheta_3\left(\frac{\pi}{2K}[x_0 - iK']\right)}{\vartheta_2\left(\frac{\pi}{2K}x_0\right)} \frac{\vartheta_4\left(\frac{\pi}{2K}[x - x_0]\right)}{\vartheta_4\left(\frac{\pi}{2K}x\right)} e^{-i\bar{Q}x}. \quad (\text{B7})$$

This is an alternative representation for the solution (B3),³¹ and produces Eq.(24). The case of the optic branch ($x_0 = i\alpha$) is considered by a similar way.

The transformation of the Floquet index for the acoustic branch is carried out as follows. By noticing that

$$\begin{aligned} & Z(i\alpha + K - iK') \\ &= Z(i\alpha) + Z(K - iK') - \text{sn}(i\alpha)\text{dc}(i\alpha) \\ &= Z(i\alpha) + i \frac{KE' + K'E - KK'}{K} - \text{sn}(i\alpha)\text{dc}(i\alpha) \\ &= i \frac{\pi}{2K} - iZ(\alpha, \kappa') - i\pi \frac{\alpha}{2KK'}, \end{aligned}$$

where we used the Jacobi's imaginary transformations and the Legendre's relation $KE' + K'E - KK' = \pi/2$. Therefore, we have

$$\bar{Q}(\bar{\alpha}) = Q(\alpha) = \frac{\pi\alpha}{2KK'} + Z(\alpha, \kappa').$$

The same transformation for the optic mode ($\bar{\alpha} = i\alpha - iK'$) yields

$$Q(\alpha) = \frac{\pi\alpha}{2KK'} + Z(\alpha, \kappa') + \text{dn}(\alpha, \kappa') \frac{\text{cn}(\alpha, \kappa')}{\text{sn}(\alpha, \kappa')}. \quad (\text{B8})$$

By the same manner, the corresponding spectrum is parametrized as

$$\bar{A}_{\bar{\alpha}} = \frac{1}{\kappa^2} \text{dn}^2 \bar{\alpha} = A_{\alpha} = \begin{cases} \frac{\kappa'^2}{\kappa^2} \text{sn}^2 \alpha & (\text{acoustic}) \\ \frac{1}{\kappa^2 \text{sn}^2 \alpha} & (\text{optic}) \end{cases}.$$

Now, we briefly review the origin of the band structure.³⁰ In the limit $\kappa \rightarrow 1$, the Lamé equation reduces to the Schrödinger equation,

$$\frac{d^2 \varphi(x)}{dx^2} + E + U_0 \text{sech}^2(\alpha x) = 0,$$

where $E = k^2(1 + A) - \ell(\ell + 1)$, $U_0 = \ell(\ell + 1)$. The potential

$$U(x) = -U_0 \text{sech}^2(\alpha x),$$

is modified Pöschl-Teller potential and for $\ell = 1$, there are one bound state and one *perfectly transmitted (reflectionless)* scattering state.⁴⁵ The band structure of the Lamé equation is understood as follows. In the limit of well separated modified Pöschl-Teller potential, the ℓ bound states give discrete levels and the scattering states give broad continuum. When the potentials form a lattice, the discrete level overlaps and the energy band may be formed. Even after the band formation, the gap between the bound level and the scattering continuum remains. Therefore, the resulting band is split into the lower acoustic band and the upper optical band.

APPENDIX C: COMPUTATION OF \mathcal{K}_{α}

We compute

$$\begin{aligned} \mathcal{K}_{\alpha} &= 2 \int_0^L dx \text{dn}(x, \kappa) u_{\alpha}(x) \\ &= 2N(\alpha) \int_0^L dx \text{dn}(x, \kappa) \frac{\vartheta_4\left(\frac{\pi}{2K}(x - x_0)\right)}{\vartheta_4\left(\frac{\pi}{2K}x\right)} e^{-iQx}, \end{aligned}$$

with $x_0 = i\alpha + K$. Noting that $\text{dn}(x, \kappa) \frac{\vartheta_4\left(\frac{\pi}{2K}(x - x_0)\right)}{\vartheta_4\left(\frac{\pi}{2K}x\right)}$ has a period $2K$, we perform the Fourier decomposition,

$$\text{dn}(x, \kappa) \frac{\vartheta_4\left(\frac{\pi}{2K}(x - x_0)\right)}{\vartheta_4\left(\frac{\pi}{2K}x\right)} = \sum_l \gamma_l e^{i\frac{\pi l}{K}x},$$

where the coefficients are evaluated as

$$\gamma_l = \frac{1}{2K} \int_{-K}^K dx \, \text{dn}(x, \kappa) \frac{\vartheta_4\left(\frac{\pi}{2K}(x-x_0)\right)}{\vartheta_4\left(\frac{\pi}{2K}\tilde{x}\right)} e^{-i\frac{\pi x}{K}l}.$$

Then, we have

$$\begin{aligned} \mathcal{K}_\alpha &= 2 \int_0^L \text{dn}(x, \kappa) u_\alpha(x) dx \\ &= 2N(\alpha) L \sum_l \gamma_l \delta_{Q, \frac{\pi}{K}l}. \end{aligned}$$

Within the acoustic branch ($0 \leq |Q| \leq \frac{\pi}{2K}$), only $Q = 0$ ($\alpha = 0$) contributes to \mathcal{K}_α . Eventually, the orthogonality condition (38) of a denumerable basis enforces that there is no contribution of the term with $l \neq 0$. $\Lambda_{\alpha=0}(x) = \sqrt{\frac{K(\kappa)}{LE(\kappa)}} \text{dn}(x, \kappa)$. Therefore we have $\mathcal{K}_\alpha = \delta_{\alpha,0} \mathcal{K}_0$, where

$$\begin{aligned} \mathcal{K}_0 &= 2 \sqrt{\frac{K(\kappa)}{E(\kappa)L}} \int_0^{\bar{L}} \text{dn}^2(x, \kappa) dx \\ &= 2 \sqrt{\frac{E(\kappa)}{K(\kappa)L}}, \end{aligned}$$

where we used the relation $E(\kappa) = \int_0^{K(\kappa)} \text{dn}^2(x, \kappa) dx$.

APPENDIX D: INERTIAL MOTION OF BLOCH WALL

We here discuss the relevance of the present formulation to the Döring-Becker-Kittel mechanism.^{16,17,18} We consider a conventional Bloch wall in ferromagnets, where the magnetization rotates through the plane of the wall. The wall size is determined by the exchange energy cost and the anisotropy energy that amount to

$$\sigma = \frac{\pi^2 JS^2}{Na_0^2} + KNa_0, \quad (\text{D1})$$

where N is the number of spins inside the wall. Minimizing this energy leads to the wall size $l_{\text{Bloch}} = \pi\sqrt{JS^2/Ka_0}$ with K denoting the anisotropy energy. Now, let us consider the Bloch wall formed along the x -axis and spins are confined to the yz -plane that winds 180° . Döring proposed that the translation of the domain wall is driven by the appearance of the local demagnetization field H_x inside the wall that violates the condition $\nabla \cdot \mathbf{M} = 0$, i.e. $H_x = -4\pi [M_x - M_x(\infty)]$, and causes

the precessional motion of the magnetization within the yz -plane. Then, the corresponding Larmor frequency amounts to $\omega_L = \dot{\varphi} = \gamma H_x$, where γ is a gyromagnetic ratio. On the other hand, in the steady movement of the wall, $\dot{\varphi} = -(\partial_x \varphi) V$, with V being the velocity, and consequently we have

$$H_x = -\gamma^{-1} (\partial_x \varphi) V. \quad (\text{D2})$$

The excess of magnetization energy

$$\Delta W = \frac{1}{8\pi} \int_{-\infty}^{\infty} H_x^2 dx = \frac{V^2}{8\pi\gamma^2} \int_{-\infty}^{\infty} \left(\frac{\partial \varphi}{\partial x} \right)^2 dx$$

gives the energy stored in the moving wall. Taking the form $\Delta W = M_{\text{Döring}} V^2/2$ the inertial mass of the wall first proposed by Döring¹⁶ is introduced

$$M_{\text{Döring}} = \frac{1}{4\pi\gamma^2} \int_{-\infty}^{\infty} \left(\frac{\partial \varphi}{\partial x} \right)^2 dx. \quad (\text{D3})$$

The explicit form $(\partial \varphi / \partial x)^2$ depends on kind of domain walls, their orientation around crystallographic axes, for example

$$M_{\text{Döring}} = \frac{1}{4\pi\gamma^2} \sqrt{K/J}$$

for 180-degree domain wall parallel to crystallographic plane (100). Taking into account that $\gamma = 1.84 \times 10^7$ [(Oe · s)⁻¹] this yields in the case of Fe

$$M_{\text{Döring}} \simeq 10^{-10} [\text{g/cm}^2].$$

From Eq. (D2) it stems that

$$M_x = -\frac{1}{4\pi} H_x = \frac{1}{4\pi\gamma} (\partial_x \varphi) V$$

provided $M_x(\infty) = 0$. This equation should be compared with Eq.(58) rewritten in the form

$$m(\bar{x}) \simeq -\frac{g\mu_B \hbar}{2Ja_0q_0} (\partial_{\bar{x}} \varphi) \dot{X}.$$

We see that $m(\bar{x})$ may be interpreted as the demagnetization field and the physical Hamiltonian (50) may be regarded as the energy cost associated with the demagnetization process.

¹ I. Žutić, J. Fabian, and S. Das. Sarma, Rev. Mod. Phys. **76**, 323 (2004) and references therein.

² J. C. Slonczewski, J. Magn. Magn. Mater. **159**, L1 (1996).

³ L. Berger, Phys. Rev. **B54**, 9353 (1996).

⁴ M. D. Stiles and A. Zangwill, J. Appl. Phys. **91**, 6812 (2002).

⁵ M. D. Stiles and A. Zangwill, Phys. Rev. **B66**, 014407 (2002).

- ⁶ G. Tataru and H. Kohno, Phys. Rev. Lett. **92**, 086601(2004).
- ⁷ Y. Aharonov and A. Stern, Phys. Rev. Lett. **69**, 3593 (1992).
- ⁸ Ya. B. Bazaliy, B. A. Jones, and S.-C. Zhang, Phys. Rev. B **57**, R3213 (1998).
- ⁹ E. I. Rashba, Sov. Phys. Solid State **2**, 1109 (1960).
- ¹⁰ S. Murakami, N. Nagaosa, and S. C. Zhang, Science **301**, 1348 (2003).
- ¹¹ J. Sinova, D. Culcer, Q. Niu, N. A. Sinitsyn, T. Jungwirth, and A. H. MacDonald, Phys. Rev. Lett. **92**, 126603 (2004).
- ¹² P. Bruno and V. K. Dugaev, Phys. Rev. B **72**, 241302(R) (2005).
- ¹³ E. I. Rashba, J. Superconductivity, **18**, 137 (2005).
- ¹⁴ I.A. Fomin, Physica **B169**, 153 (1991); G. E. Volovik, arXiv:cond-mat/0701180.
- ¹⁵ L. D. Landau and E. M. Lifshitz, Fluid Mechanics (Pergamon, Oxford, 1984)
- ¹⁶ W. Döring, Zeits. f. Naturforschung 3a, 374 (1948).
- ¹⁷ R. Becker, Proceedings of the Grenoble Conference, July (1950).
- ¹⁸ C. Kittel, Phys. Rev. **80**, 918 (1950).
- ¹⁹ I. E. Dzyaloshinskii, J. Phys. Chem. Solids **4**, 241 (1958).
- ²⁰ J. Kishine, K. Inoue, and Y. Yoshida: Prog. Theoret. Phys., Supplement **159**, 82 (2005).
- ²¹ I.G. Bostrem, J. Kishine, and A. S. Ovchinnikov, Phys. Rev. **B 77**, 132405 (2008).
- ²² Izumov Yu. A., Naish V. E. and Ozerov R. P., *Neutron Diffraction of Magnetic Materials*, Consulting Bureau, New York (1991).
- ²³ O. V. Kovalev, *Representations of the Crystallographic Space Groups* Edition 2 (Gordon and Breach Science Publishers, Switzerland, 1993).
- ²⁴ T. Moriya and T. Miyadai, Solid State Commun. **42** (1982), 209.
- ²⁵ B. Roessli, J. Schefer, G. A. Petrakovskii, B. Ouladdiaf, M. Boehml, U. Staub, A. Vorotinov, and L. Bezmaternikh, Phys. Rev. Lett. **86** (2001), 1885.
- ²⁶ Y. Kousaka, S. Yano, J. Kishine, Y. Yoshida, K. Inoue, K. Kikuchi, and Jun Akimitsu, J. Phys. Soc. Jpn. **76**, 123709 (2007).
- ²⁷ L. L. Liu, Phys. Rev. Lett. **31**, 459 (1973).
- ²⁸ J. Scalapino, Y. Imry, and P. Pincus, Phys. Rev. **B 11**, 2042 (1975).
- ²⁹ I. E. Dzyaloshinskii, Sov. Phys. JETP **19**, 960 (1964); Sov. Phys. JETP **20**, 665 (1965).
- ³⁰ B. Sutherland, Phys. Rev. A **8**, 2514 (1973).
- ³¹ Yu. A. Izyumov and V. M. Laptev, JETP **62**, 755 (1985).
- ³² D. N. Aristov and A. Luther, Phys. Rev. **B 65**, 165412 (2002).
- ³³ R. J. Elliott and R. V. Lange, Phys. Rev. **152**, 235 (1966).
- ³⁴ E. T. Whittaker and G. N. Watson, *A Course of Modern Analysis* (Cambridge University Press, New York, 1927).
- ³⁵ N. H. Christ and T. D. Lee, Phys. Rev. D **12**, 1606 (1975).
- ³⁶ R. Rajaraman, *Solitons and Instantons; An Introduction to Solitons and Instantons in Quantum Field Theory*, North-Holland, Amsterdam and New York, (1982).
- ³⁷ J. Heurich and J. König, and A. H. MacDonald, Phys. Rev. **B68**, 064406 (2003).
- ³⁸ P. Chandra, P. Coleman and A. I. Larkin, J. Phys.: Condens. Matter **2**, 7933 (1990).
- ³⁹ F. Schütz, P. Kopietz, and M. Kollar, Eur. Phys. J. B **41**, 557 (2004).
- ⁴⁰ J. Xiao, A. Zangwill, and M. D. Stiles, Phys. Rev. B **73**, 054428 (2006). Nonequilibrium spin currents in this work are considered for free-electron Stoner model for systems with continuously nonuniform magnetization.
- ⁴¹ V. I. Fedorov, A. G. Gukasov, V. Kozlov, S. V. Maleyev, V. P. Plakhty, I. A. Zobkalo, Phys. Lett. A **224**, 372 (1997).
- ⁴² B. Hu and J. Tekić, Phys. Rev. Lett. **87**, 035502 (2001).
- ⁴³ S. Chikazumi, *Physics of Ferromagnetism*, Oxford, New York (1996).
- ⁴⁴ S. Flügge, *Practical Quantum Mechanics*, Springer-Verlag, Berlin, 1971.
- ⁴⁵ L.D. Landau and E.M. Lifshitz, *Quantum Mechanics*, Pergamon, London, (1958).